Characterization of Saharan and Sahelian dust sources based on geochemical and radiogenic isotope signatures

D. Guinoiseau, S. P. Singh, S. J. G. Galer, W. Abouchami, R. Bhattacharyya, K. Kandler, C. Bristow, M. O. Andreae

Quaternary Science Reviews 293 (2022) 107729

Contents lists available at ScienceDirect

Quaternary Science Reviews

journal homepage: www.elsevier.com/locate/quascirev

Invited paper

Characterization of Saharan and Sahelian dust sources based on geochemical and radiogenic isotope signatures

D. Guinoiseau [a, b], S.P. Singh [b, c, *], S.J.G. Galer [b], W. Abouchami [d], R. Bhattacharyya [c], K. Kandler [e], C. Bristow [f], M.O. Andreae [b, g, h]

[a] Université Paris-Saclay, CNRS, GEOPS, 91405 Orsay, France
[b] Max Planck Institute for Chemistry, Climate Geochemistry Department, Mainz, Germany
[c] Department of Earth and Environmental Sciences, Indian Institute of Science Education and Research Bhopal, Bhopal, 462066, Madhya Pradesh, India
[d] Institut für Geologie und Mineralogie, Universität zu Köln, Köln, Germany
[e] Technical University Darmstadt, Darmstadt, Germany
[f] Department of Earth and Planetary Sciences, Birkbeck University of London, London, UK
[g] Scripps Institution of Oceanography, University of California San Diego, La Jolla, CA, USA
[h] Department of Geology and Geophysics, King Saud University, Riyadh, Saudi Arabia

ARTICLE INFO

Article history:
Received 18 March 2022
Received in revised form
24 August 2022
Accepted 24 August 2022
Available online 8 September 2022

Handling Editor: Dr Giovanni Zanchetta

Keywords:
North african soils
Rare-earth element pattern
Sr-Nd-Pb radiogenic Isotopes
Mineral dust provenance
Isotope fingerprinting
Atlantic dust transport

ABSTRACT

Mineral dust can significantly impact climate and biogeochemical cycles on Earth. To understand dust provenance, an accurate characterization of dust sources and emission regions is required. In this study, we combine rare-earth element patterns, elemental ratios, and radiogenic Sr-Nd-Pb isotopes to discriminate dust sources from key regions in North Africa responsible for ~55% of the total dust load emitted annually on Earth. This new dataset, based on fifty-nine analyses of deflatable fine soil material, improves our current knowledge about North African dust sources, especially those underrepresented in Saharan-Sahelian regions. Six potential source areas (PSA) – Libya-Algeria-Mali (PSA_{LAM}), Libya-Egypt (PSA_{LE}), Bodélé Depression (PSA_{BD}), Mali Center (PSA_{MC}), West African Coast (PSA_{WAC}) and Mauritania (PSA_{Ma}) – are defined based on several lithogenic tracers as well as on the geological subdivision of North African geological provinces, providing a unique chemical and isotope fingerprint for each PSA. For example, the PSA_{BD} – the main dust activation area in North Africa – is clearly distinguished from western African sources using Pb isotopes. Major elements show a large variability within each PSA and are not alone diagnostically useful. Comparison of the newly defined PSA with aerosols collected in remote locations over the North Atlantic shows that their sources are predominantly from western African regions (PSA_{LAM} and PSA_{WAC}). Bodélé-derived dust has a limited impact on the bulk dust transported over the tropical North Atlantic, regardless of the season and altitude of dust transport. The low impact of the Bodélé Depression can be explained by a high deposition rate (wet and dry) of aerosols along its southwestward trajectory. A detailed analysis of dust collected over South America during winter will be essential to confirm this observation at a global scale. The present dataset can be efficiently used to track modern dust emissions as well as their changes at the scale of glacial/interglacial cycles or during the development of African Humid Periods as stored in sedimentary archives.

1. Introduction

Dust plays an important role in shaping the Earth system through its physical, chemical and biological influence (Goudie and Middleton, 2006; Mahowald et al., 2005; Prospero and Mayol-Bracero, 2013; Shao et al., 2011; Tegen, 2003). According to the most recent estimates, North Africa is the principal global source, responsible for ~55% of the 1536 Tg total dust emitted annually (Ginoux et al., 2012). Deflated Saharan-Sahelian dusts are blown to the west by the prevailing easterlies, across the tropical Atlantic Ocean towards North America, the Caribbean, and South America depending on the seasonal position of the Inter-Tropical

* Corresponding author. Department of Earth and Environmental Sciences, Indian Institute of Science Education and Research Bhopal, Bhopal, 462066, Madhya Pradesh, India.
E-mail address: satinder@iiserb.ac.in (S.P. Singh).

https://doi.org/10.1016/j.quascirev.2022.107729

Convergence Zone (ITCZ) (Engelstaedter and Washington, 2007; Prospero et al., 1981, 2014). Along this route, a large proportion of these atmospheric aerosols accumulate in the surface ocean by dry and wet deposition, contributing essential micronutrients and leading to enhanced primary productivity and biological blooms in the oligotrophic tropical Atlantic (van der Does et al., 2021). The quantity of dust transported has been continually refined using ever-improving satellite observations (Ben-Ami et al., 2010, 2012; Yu et al., 2015a, 2018). Radiogenic isotope fingerprinting of filter-collected aerosols along the Atlantic transport pathway to the Cape Verde and Caribbean islands has significantly improved our knowledge of the most important North African sources involved in the outflow (Bozlaker et al., 2018; Jewell et al., 2020; Kumar et al., 2014, 2018; Pourmand et al., 2014; van der Does et al., 2018).

The significance of African-sourced dust as a "fertilizer" of Caribbean and Amazonian ecosystems (Reichholf, 1986; Swap et al., 1992) is still an ongoing debate (Abouchami et al., 2013; Nogueira et al., 2021; Prospero et al., 2020; Yu et al., 2015b), even if measurable inputs of key nutrients, such as Fe or P, have been well documented in South American aerosols (Barkley et al., 2019; Moran-Zuloaga et al., 2018; Rizzolo et al., 2017). The impact of Saharan dust on the biogeochemical balance of nutrients in the Caribbean was suggested on the basis of trace and rare-earth elements (Muhs et al., 2007) and more recently, using radiogenic Sr and Nd isotopes (Dessert et al., 2020). However, an averaged "Saharan dust" signature was used in the latter study, although potential source areas (hereafter denoted as PSA) across the Sahara are known to be geochemically and mineralogically diverse (Formenti et al., 2011; Scheuvens et al., 2013), which can contribute variably to the dust budget at a given location depending on the season (Kumar et al., 2018). Additionally, their different chemical and mineralogical compositions can lead to variations in the relative exported nutrient fluxes. Thus, a better characterization of these North African PSA is crucial for their reliable use in provenance and biogeochemical studies.

The Bodélé Depression in Chad and the El Djouf Desert in Western Sahara, are currently the two largest dust emitting sources in North Africa (Prospero et al., 2002). Dust suspension from these source regions is mainly due to saltation and auto abrasion processes (Bristow et al., 2009; Bristow and Moller, 2018; Giles, 2005; Koren et al., 2006). Dust transport to higher altitudes for longer-range transport is a relatively well understood process. Here, emission is often a diurnal phenomenon in which strong low-level jets, which have lowered in height during the night, interact with convective instabilities formed by surface heating in the early morning (Tegen et al., 2006; Todd et al., 2007, 2008; Washington and Todd, 2005; Washington et al., 2006a, 2006b). Satellite imagery is routinely filtered to selectively visualize atmospheric dust density (but not its altitude), enabling source areas in the Saharan-Sahelian region to be spotted and the dust-emitting events to be tracked spatially over time (Ashpole and Washington, 2012, 2013a, b; Bakker et al., 2019; Klose et al., 2010; Schepanski et al., 2017; Schepanski et al., 2009a; Schepanski et al., 2009b). Additionally, information about dust altitudes can be obtained by LIDAR measurements (Ansmann et al., 2017; Haarig et al., 2019; Kumar et al., 2018; Rittmeister et al., 2017).

The recent study by Bakker et al. (2019) captured the ten largest dust events during two winter seasons (December to February 2015–16 and 2016–17) and demonstrated that (1) alluvial deposits and paleolake environments are responsible for most of the dust emissions (~53 and ~41%, respectively), while (2) ~45% of the total budget is associated with the Bodélé Depression area. However, the end of the winter season was not evaluated (due to cloud cover), likely underestimating West African sources, which are more active between March and May, especially in the El Djouf Desert region, which covers northeastern Mauritania and northwestern Mali (Kumar et al., 2018; Yu et al., 2018).

The first comprehensive definition of North African PSA was based on a summary of satellite observations along with mineralogical, elemental and/or Sr and Nd isotope measurements (Formenti et al., 2011; Scheuvens et al., 2013). Although these studies provided a means for dust source identification in North Africa, a re-evaluation and refinement of the six distinct PSA is warranted by the need to identify a unique geochemical and isotopic signature for each PSA. Recently, Jewell et al. (2020) using a combination of Sr and Nd isotopes, dust source activity and new set of samples from the Bodélé Depression and North Sudan regions delimited only three main dust sources: Western, Central and Eastern regions of North Africa. However, these three PSA are broad geographically, and the important El Djouf Desert source (Mali-Algeria) – the second-largest dust emission area after the Bodélé – is inadequately resolved within their "Western" PSA.

In view of the variability in mineral and chemical composition within individual PSA, the combination of four lithogenic tracers - radiogenic Sr, Nd, and Pb isotopes, and rare-earth element (REE) patterns - provides a powerful discriminant for identifying dust sources. Such an approach has been used successfully to investigate the provenance of dust at the Cape Verde Islands and in the Caribbean at Barbados (Kumar et al., 2018; Pourmand et al., 2014).

In this study, we present chemical (including REE patterns) and radiogenic Pb, Sr and Nd isotope compositions of fine deflatable soil material ($\lesssim$ 20 μm) from the Sahara and Sahel regions of North Africa. Our results on the effect of grain-size fractionation on radiogenic Sr, Nd, and Pb isotopes show that the isotopic composition of bulk soils are biased by mineralogical and/or grain-size sorting effects, in agreement with previous studies (Aarons et al., 2013; Chen et al., 2007; Dasch, 1969; Feng et al., 2010; Grousset and Biscaye, 2005; Meyer et al., 2011). Therefore, we opted to use the fine soil fraction as representative of the source of emitted dust. Our study aims to geochemically/isotopically demarcate under-explored active dust emitting regions by providing new Pb isotope data, which remain relatively scarce in the literature, and by complementing the current literature Sr–Nd isotope dataset of sediments and dusts from the West African Coast and the Bodélé Depression (Abouchami et al., 2013; Gross et al., 2016; Grousset and Biscaye, 2005; Grousset et al., 1998; Hamelin et al., 1990; Jewell et al., 2020; Kumar et al., 2014; Revel et al., 2010; Zhao et al., 2018). Using our new comprehensive and systematic isotope and trace element dataset combined with available literature data, we identify six distinct PSA in the North African region – these provide an important framework for locating present dust "hotspots", tracking dust transport pathways and fingerprinting past dust sources archived in Quaternary sedimentary records.

2. Materials and methods

2.1. Sample selection

Bulk soil samples were from a collection known as the "Mainz Sandbank", comprising samples from across the Sahara-Sahel region collected on multiple field trips from 1970 onwards, stored in 1-L LDPE bottles at room temperature. Most targeted samples were chosen from locations known to contribute to the westward African dust outflow and a few samples were selected from the north-eastern Sahara (Fig. 1). Additional samples with the prefix "CH" consist essentially of dune sands and sediments collected during the 2005 BodEx campaign from the Bodélé Depression (Washington et al., 2006a), and for which P and Fe contents are available (Hudson-Edwards et al., 2014; Moskowitz et al., 2016). Five samples analyzed here from the BodEx collection were also

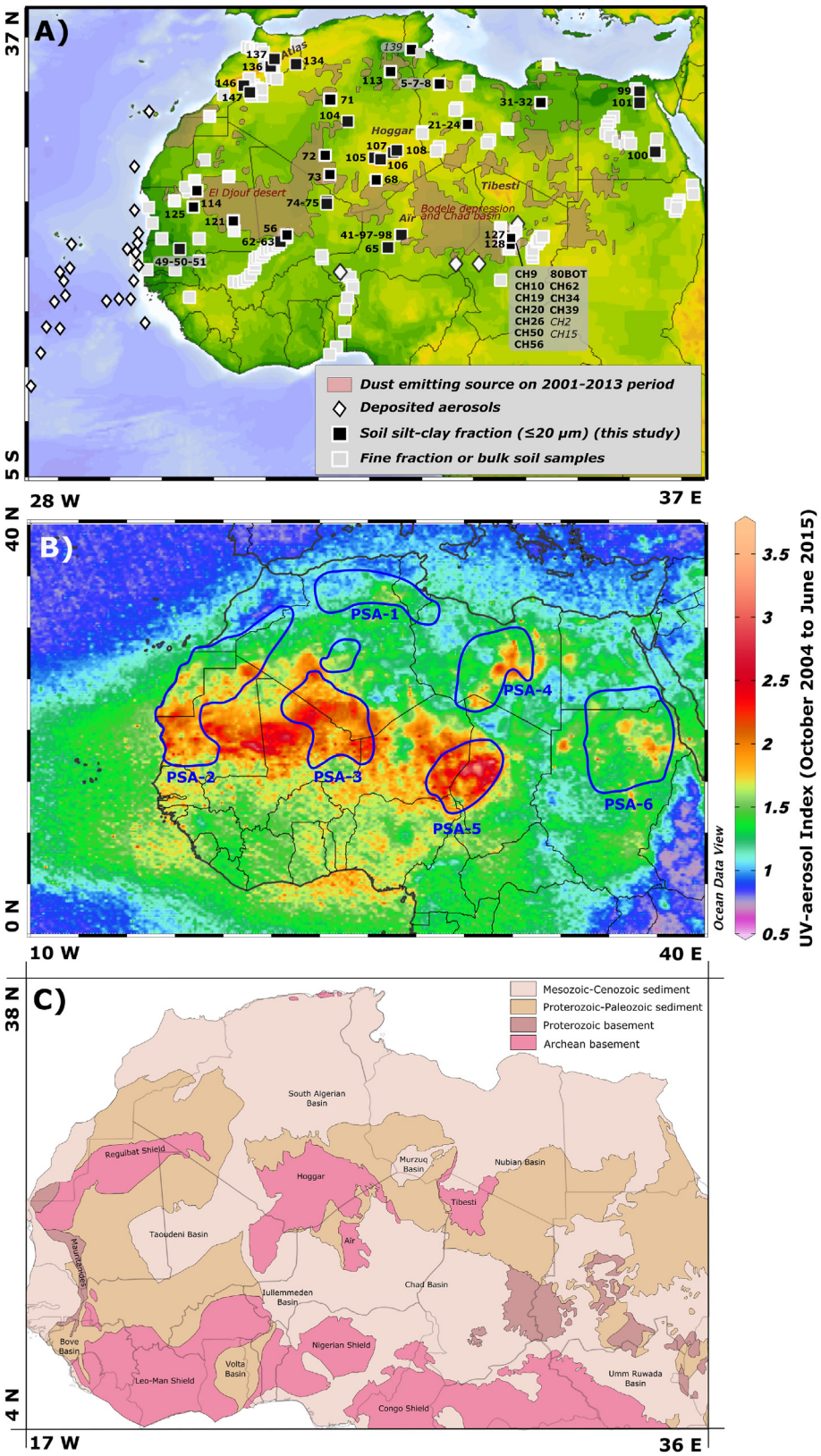

Fig. 1. A) Map of sample locations and dust emitting sources. Marked areas represent the dust emission sources determined using MISR satellite observations between 2001 and 2013 (Yu et al., 2018). White diamonds and grey squares correspond to deposited aerosols and fine fraction/bulk soil samples reported in the literature, respectively (Aarons et al., 2013; Abouchami and Zabel, 2003; Gross et al., 2016; Grousset and Biscaye, 2005; Grousset et al., 1992, 1998; Hamelin et al., 1990; Jewell et al., 2020; Kumar et al., 2014, 2018; Meyer et al., 2011; Pourmand et al., 2014; Revel et al., 2010; Rognon et al., 1996; Skonieczny et al., 2011, 2013; van der Does et al., 2018; Zhao et al., 2018). Italic-labeled samples refer to outliers (see 3.3 section for further details). **B) Map of potential source areas (PSA) and UV-aerosol index in North Africa.** The definition of the six PSA is based on Formenti et al. (2011), whereas the UV-aerosol index map is based on Aura-OMI satellite data between October 2004 and June 2015. The agreement between the geographic extension of PSA and UV-AI is not optimal, especially for PSA2 and PSA3. **C) Geological map of North Africa adapted from Ye et al. (2017).**

measured for Sr and Nd isotopes by Jewell et al. (2020) and are in good agreement (see Fig. S1). Lead isotope compositions of HBr leachates and residues of free-fall atmospheric dusts from Chad and Niger, for which bulk, unleached isotope analyses are available (see Abouchami et al., 2013), were also measured.

2.2. Granulometric sorting and selective leaching experiments

In order to assess the effect of grain size and sequential leaching on Sr, Nd and Pb isotopes, four samples were selected from Mali (S-62 & S-63) and Morocco (S-136 & S-147), which are characterized by distinct bedrock ages, soil types, and elevations. The finer fractions of the bulk soils ($\lesssim$20 μm, hereafter termed "SC") were specifically targeted, as they constitute the deflatable material potentially emitted as dust. Different grain size fractions were extracted from the bulk soils based on differential gravitational settling in water columns according to Stokes' law, following a procedure modified after Gee and Or (2002). These fractions are labeled: fine clay, "FC" ($\lesssim$1 μm), clay, "C" ($\lesssim$2 μm), silt, "St" (2 μm $\lesssim$ St $\lesssim$ 20 μm; containing < 1% clay), and silt-clay, "SC" ($\lesssim$20 μm). A detailed description along with a schematic illustration (Fig. S2) of the physical/chemical steps involved in our methodology for obtaining the various size fractions is reported in the Appendix (Text S1).

2.3. Concentration and isotope analysis

For elemental and radiogenic isotope analyses, the different soil fractions (FC, C, St, HBr leachate and residue) of the four Malian and Moroccan soils (Tables S3 and S4) as well as all SC aliquots (Tables S1 and S5), corresponding to ~10–20 mg of lithic materials, were dried and digested in a mixture of 27 M HF and 16 M HNO_3. Between ~0.6 and 6.0 mg of the digested SC fraction were used to determine the major and trace element composition using an Agilent 7900 quadrupole ICP-MS instrument with 2.5% HNO_3 (distilled with a trace of HF) as eluent. Calibration standards were prepared by dilution from certified reference solutions supplied by Inorganic Ventures. International reference materials (basalts BHVO-2 and BCR-2) were analyzed during each measurement session, and the data agree within ±10% of the recommended reference concentrations (Jochum et al., 2016) – see Table S2. The new Bodélé Depression samples were homogenized by manual grinding in a pre-cleaned agate mortar before digestion of the bulk soil material.

Sequential column chemistry for purification of Sr, Nd, and Pb has been described in detail elsewhere (Abouchami et al., 2013; Kumar et al., 2014). Strontium, Nd, and Pb isotope compositions were measured by thermal ionization mass spectrometry (TIMS Triton, ThermoFisher). Lead was loaded on rhenium filaments with a colloidal silica gel, while Sr and Nd were loaded on tungsten filaments between two micro-drops of TaF_5 solution. The $^{87}Sr/^{86}Sr$ was corrected for instrumental mass bias by normalizing to $^{86}Sr/^{88}Sr$ of 0.1194. The Nd isotope compositions were measured as the NdO^+ ion and the $^{143}Nd/^{144}Nd$ ratios, after oxygen stripping, were corrected for mass bias using $^{146}Nd/^{144}Nd$ of 0.7219. Replicate measurements of SRM 987 and La Jolla standards yielded $^{87}Sr/^{86}Sr$ of 0.710267 ± 0.000010 (2SD, n = 22) and $^{143}Nd/^{144}Nd$ of 0.511838 ± 0.000011 (2SD, n = 16), respectively. The Pb isotope data were corrected offline for instrumental mass bias using a double (^{207}Pb–^{204}Pb) or triple (^{204}Pb–^{206}Pb–^{207}Pb) spike technique (Galer, 1999). Multiple analyses of the NIST SRM-981 standard using the triple-spike yielded $^{206}Pb/^{204}Pb$, $^{207}Pb/^{204}Pb$, and $^{208}Pb/^{204}Pb$ of 16.9436 ± 0.0013, 15.5012 ± 0.0018, and 36.7308 ± 0.0042 (2SD, n = 22), respectively. These values agree within uncertainties with those obtained using the double-spike technique (16.9446 ± 0.0031, 15.5023 ± 0.0045, and 36.7348 ± 0.0087; 2SD, n = 14).

3. Results

3.1. Sequential extraction

The Sr, Nd, and Pb isotope compositions of the various aluminosilicate size-fractions extracted from Moroccan and Malian SC fractions are reported in Table S3 and Fig. 2. Malian soils present distinctive radiogenic Sr and Pb isotope ratios and unradiogenic ε_{Nd} compared with Moroccan soils, in line with their contrasting geology. While the ε_{Nd} are nearly constant, there are Pb isotope differences between SC, clay, and fine clay fractions, with the silt fraction being significantly different. The silt fractions have less radiogenic Nd and Pb isotope ratios in Malian soils and have more radiogenic Pb isotope signatures in Moroccan soils (Fig. 2). For $^{87}Sr/^{86}Sr$, the main difference is seen between unradiogenic ratios in the SC soil and radiogenic $^{87}Sr/^{86}Sr$ in the other fine fractions, likely due to the purification process.

Strontium, Nd and Pb isotope compositions of the 0.5 M HBr leachate and residue of the bulk SC fractions (L-SC, R–SC) are reported in Table S4 and Fig. S3. Lead isotope ratios measured on residues (R-samples) following 0.5 M HBr leaching of free-fall dust samples are also reported (Table S4). For all isotope systems, the leachates are less radiogenic than the silicate residue, this effect being more marked for $^{87}Sr/^{86}Sr$ and Pb isotope ratios than for ε_{Nd}.

3.2. Chemical and radiogenic isotope characterization of soil samples

The first definition of North African PSA proposed by Formenti et al. (2011) and Scheuvens et al. (2013) was based on a combination of chemical and mineralogical proxies. Recent studies using satellite imagery show that some important regions (e.g., the El-Djouf Desert) were still lacking an accurate characterization due to poor spatial coverage inherent with any single-spot soil sampling. Additionally, proxies like elemental ratios or mineralogical compositions are not sufficiently diagnostic of an individual PSA (Formenti et al., 2011, 2014). In this study, we attempt to refine the signature of individual North African PSA by analyzing 59 new soils collected from the majority of the potential dust-emitting regions. In combination with the widely used radiogenic Sr–Nd isotopes in previous studies, we make use of radiogenic Pb isotope compositions, REE patterns, and selected elemental ratios to uniquely fingerprint the PSA. The Sr-Nd-Pb isotope dataset and chemical compositions of the fine soil fractions (SC) are presented in Tables S1 and S5, respectively. Amongst the 59 SC soil fractions, highly variable and generally anticorrelated $^{87}Sr/^{86}Sr$ and ε_{Nd} are observed ($^{87}Sr/^{86}Sr$: 0.708–0.729 and ε_{Nd}: 5 to −17.5, Table S1) in line with available data in literature. Important variations across the sample set are also noted for $^{206}Pb/^{204}Pb$ (18.03–19.20), $^{207}Pb/^{204}Pb$ (15.58–15.78) and $^{208}Pb/^{204}Pb$ (37.96–39.70).

3.3. Data filtering

Before using lithogenic tracers for fingerprinting North African PSA, the dataset as a whole was filtered to remove possible outliers. These outliers may consist of samples that are simply not representative of the local geology or have been affected by incongruent weathering or anthropogenic contamination. Either way, such samples exert an unnecessary bias in trying to delimit the compositions of the dust-emitting regions, and we considered it imperative to identify such outliers objectively. In total, five of the fifty-nine soils were excluded from further consideration.

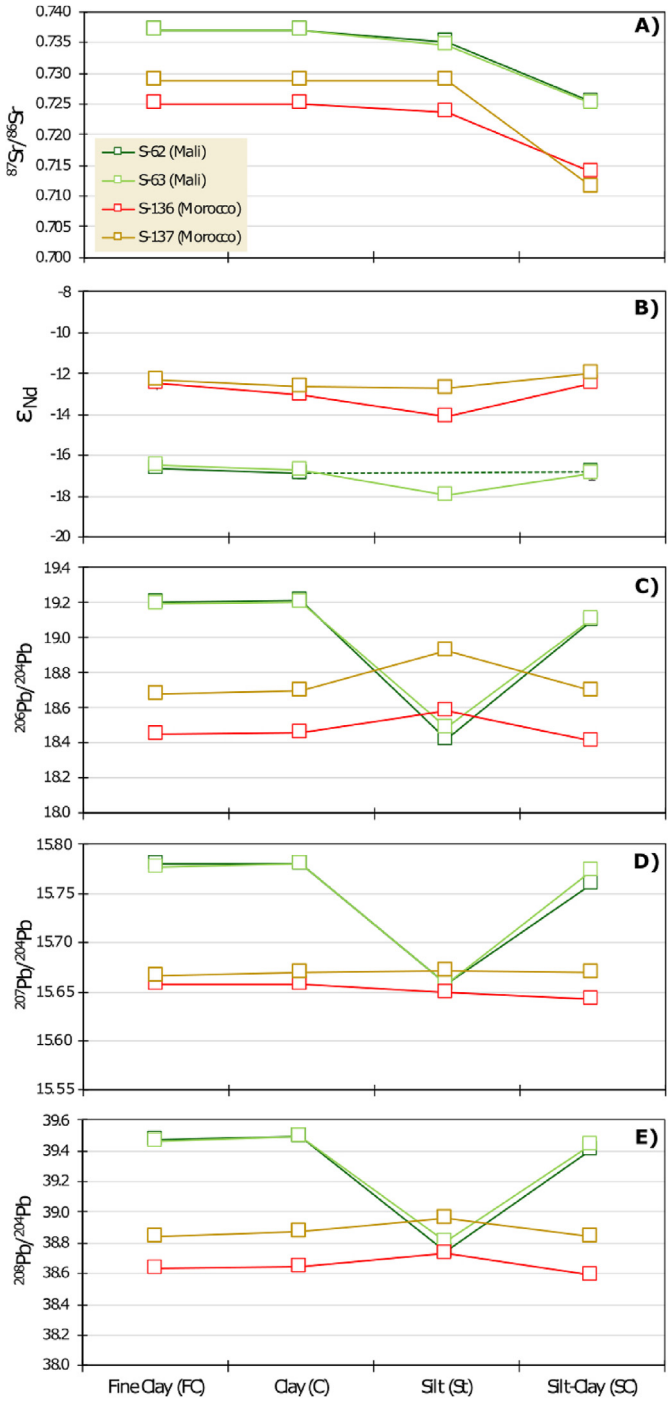

Fig. 2. Radiogenic isotope signatures (A: $^{87}Sr/^{86}Sr$; B: ε_{Nd}; C: $^{206}Pb/^{204}Pb$; D: $^{207}Pb/^{204}Pb$ and E: $^{208}Pb/^{204}Pb$) in the size-fractions separated using the protocol described in section 2.2. Contrary to other size fractions, the silt-clay fraction did not undergo chemical leaching of carbonate, organic matter, and oxides/hydroxides. Uncertainties (reported as 2SD) are smaller than symbols.

Tunisian sample SC-139 is a salt-pan deposit (chott) based on its Na concentration (Table S5) and Google Earth observation and was therefore discarded. Since the evaporitic fraction overwhelmingly dominates the elemental content (particularly true for Sr and to a lesser extent for Pb), this sample was considered unlikely to be representative of the local Tunisian geology.

Samples from the Bodélé Depression were analyzed, with the geochemical and isotope data reported in Table S1 (prefix "CH"). The Bodélé Depression consists of a large variety of geological terrains, which are represented among the samples, and only some of these terrains are responsible for dust emission. Rosner's generalized ESD test for outliers at $p < 0.05$ (Rosner, 1983), implemented in *R*, was applied to the whole Bodélé population ($n = 25$, including literature data, Tables S1, S5 and S6) to identify outliers in the Nd and Pb isotope datasets. Using this statistical approach, samples CH34 and CH39 (for ε_{Nd}) and CH2 and CH15 (for Pb isotopes) were identified as outliers and excluded (Fig. S4).

Samples CH34 and CH39 are from the northern edge of the depression where the Angamma paleodelta is located draining the young volcanic Tibesti Mountains, as clearly reflected in the highly radiogenic ε_{Nd} values measured (Fig. S4). Even if this sediment source likely represents an end-member flowing into the Bodélé Depression (Jewell et al., 2020), its highly radiogenic signature is not representative of that of the average Bodélé Depression. Samples CH2 and CH15 have extreme $^{206}Pb/^{204}Pb$ ratios (>20.0, Fig. S4), with CH2 also exhibiting very radiogenic $^{208}Pb/^{204}Pb$, lying far outside the data ranges seen for North African soils as a whole. Since $^{87}Sr/^{86}Sr$ and ε_{Nd} show values in the range of signatures reported for the whole PSA_{BD} dataset (Table S1), the highly radiogenic Pb isotope composition may reflect Pb contamination, though in the opposite sense expected for anthropogenic Pb. More likely, it is the result of incongruent weathering, which preferentially leaches out and releases radiogenic Pb, as discussed by Harlavan and Erel (2002).

The five samples identified here are neither included in any of the figures nor considered further in the discussion, and are marked as outliers in the Tables.

4. How useful are REE and elemental patterns alone for PSA identification?

Based on the similarity in REE patterns, the geographic proximity of the soils to one another and the dust emission sources determined using MISR satellite observations (Fig. 1A, Yu et al., 2018), we can identify five main potential PSA: 1. West African Coast (PSA_{WAC}, largely Morocco/Mauritania/Senegal), 2. Libya/Egypt (PSA_{LE}), 3. Libya/Algeria/Mali (PSA_{LAM}), 4. Mali Center (PSA_{MC}), and 5. Bodélé Depression (PSA_{BD}). The color coding used in all figures is based on this definition of the PSA. To facilitate the comparison between the individual PSA, average UCC-normalized REE pattern are reported in Fig. S5. Samples collected within the Hoggar Mountains (SC-68, SC-105-SC-108) and at the southernmost extension of the Aïr Moutains (SC-41, SC-97 and SC-98) are not considered as representative of major PSA. Indeed, in the Hoggar and Aïr mountainous regions, coarse and non-deflatable material are predominant, and no dust activity has been documented (Fig. 1B). Exhumation of both systems only started during the Late Eocene (40-30 Ma, Ye et al., 2017) and surface sediment deposits associated with their erosion are restricted to the Iullemmeden Basin, located south of the limit of intense dust activity (Fig. 1C). While alluvial fans can potentially provide an additional source of sediments, they are unlikely, given their limited surface coverage, to be a significant dust contributor and thus, a major PSA (Fig. 1C).

The SC-65 sample from Gal in Niger does not fit any PSA based on its REE pattern and thus remains unassigned. However, in Figs. 3 and 4, SC-65 is included within the non-representative PSA panel (Hoggar and Aïr samples) based on its geographic association. The REE pattern of SC-113, as well as its Eu anomaly, $^{87}Sr/^{86}Sr$ and ε_{Nd} signatures (Table S1) are quite different from those of the other samples belonging to the PSA_{LAM}. This sample is included in the different figures but not further considered in determining the signature of this PSA. Although a few REE profiles have been

reported for North Africa (Abouchami et al., 2013; Moreno et al., 2006; van der Does et al., 2018), these analyses were performed on bulk samples only and some have insufficient accuracy to be useful (Fig. S6). A direct comparison between our fine soil fraction and these datasets is potentially misleading due to the influence of heavy mineral sorting on REE patterns, as documented in several studies (Ferrat et al., 2011; Kanayama et al., 2005; Yang et al., 2007a, 2007b). Consequently, the REE patterns of fine SC materials reported here and normalized to UCC (Upper Continental Crust; Rudnick and Gao, 2014) constitute a new consistent dataset for future provenance studies aiming at tracing North African dust emission, transport, and deposition.

The extended elemental patterns, normalized to Al and to the UCC, are plotted for each of the five potential PSA in Fig. 4. Within each PSA, chemical compositions are reasonably similar (Fig. 4), but the intra-PSA variability still remains sufficiently large that the full elemental spectra alone cannot be used reliably as a geochemical fingerprinting tool. For example, the carbonate content in both the PSA_{WAC} and PSA_{LE} is variable between samples (Fig. S7) which can significantly affect the concentrations of the alkaline-earth elements (Mg, Sr, Ca or Ba).

However, taken individually, several elemental ratios appear to uniquely fingerprint some PSA– specifically, the PSA_{WAC}, PSA_{LE} and PSA_{MC} (Fig. S8). High As/Al is found in most PSA_{WAC} samples (Fig. S8B). Here, arsenic is likely an accessory element in sulfide or iron-rich materials, consistent with numerous mining operations documented in the region (IUCN/PACO, 2012). Manganese and Zn depletions seem to be diagnostic of the PSA_{MC} even though additional measurements are obviously needed to confirm this observation (Fig. S8A).

High-field strength element ratios are also insightful as a proxy for the proportions of heavy minerals that predominantly host these refractory elements in soils. The highest Zr/Hf–Zr/ΣREE combination measured in PSA_{LE} soils may be associated with variability in the Zr/Hf ratio in zircon (Jones et al., 2017), the main carrier phase of these two elements in rocks (Fig. S8C). However, it must be borne in mind that zircon is a heavy mineral, which is unlikely to survive long-range transatlantic dust transport. Finally, Eu anomalies ($Eu^* = Eu_N/\sqrt{(Sm_N + Gd_N)}$, where N means normalized to UCC), appear promising for distinguishing PSA_{BD} ($Eu^* = 0.90 \pm 0.02$) from other PSA like PSA_{LAM} or PSA_{WAC} ($Eu^* = 0.97 \pm 0.08$ and $Eu^* = 1.05 \pm 0.07$, respectively, Table 1).

Overall, the Al-normalized element patterns generally agree with the identification of PSA based on REE patterns alone,

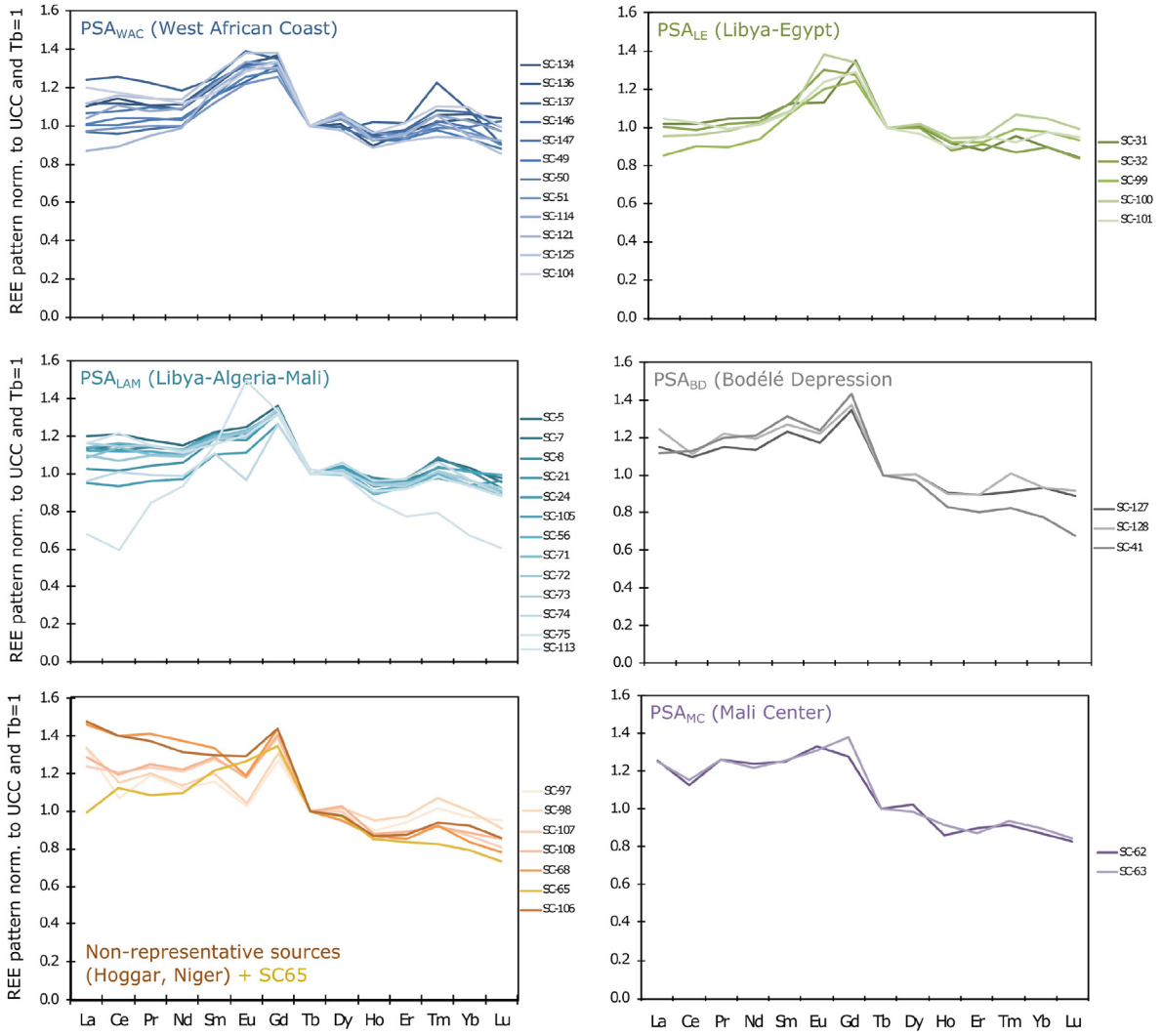

Fig. 3. UCC-normalized REE patterns for individual PSA. The UCC composition is taken from Rudnick and Gao (2014). To facilitate reading and comparison between samples, REE patterns were normalized to a nominal Tb value of 1.

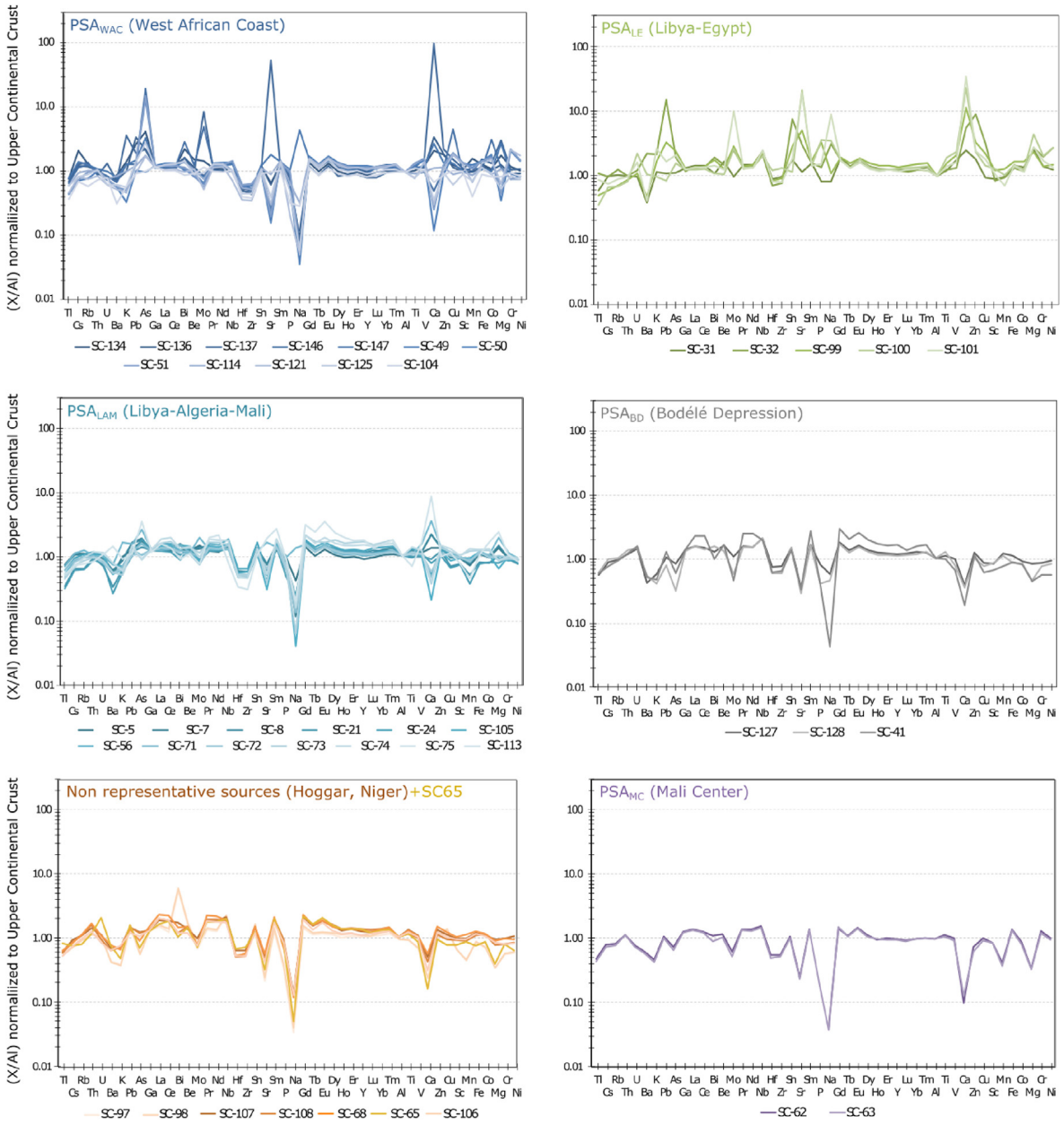

Fig. 4. Element patterns normalized to Al and to the upper continental crust (UCC) for individual PSA. Elements are ranked on the x-axis according to their respective UCC to primitive mantle ratio, from higher to lower, The UCC composition is taken from Rudnick and Gao (2014). Sample SC-65, unassigned to any PSA, is displayed along with non-representative dust sources, as in Fig. 3.

implying that the approach developed here is robust. Elemental ratios by themselves also seem typical of individual PSA, but are not sufficiently discriminant without incorporation of additional information from radiogenic Sr-Nd-Pb isotope systems.

5. Radiogenic isotopes, a discriminant tool for North African PSA

In order to use reliably the radiogenic Sr-Nd-Pb isotope signatures as a provenance tracer of "natural" mineral dust emitted from North African PSA, it is important to first exclude isotopic bias (if any) due to granulometry and mineralogy, as well as anthropogenic inputs, which can specifically alter the "natural" Pb isotope signature (Bollhöfer and Rosman, 2000; Hamelin et al., 1989).

The ε_{Nd} in the different grain size fractions (FC, C, St and SC) of Malian and Moroccan soils (Fig. 2) are comparable in each geographical region. With the exception of the silt fractions which tend to be slightly less radiogenic, the SC, C, and FC fractions exhibit similar ε_{Nd} values, implying that Nd isotopes are mainly carried by the fine mineral phases (e.g., clays) and are thus less susceptible to grain-size fractionation induced by sedimentary and aeolian transportation, in agreement with previous studies (Kumar et al., 2018 and references therein). Hence, ε_{Nd} in the Saharan-Sahel fine dust fraction reflects the material deflated in the source

Table 1
Summary of geochemical definition of North African PSA. The averages and standard deviations are based on data obtained in this study and a compilation of literature data (when available).

Name	$^{87}Sr/^{86}Sr$ (±SD)	ε_{Nd} (±SD)	$^{206}Pb/^{204}Pb$ (±SD)	$^{207}Pb/^{204}Pb$ (±SD)	$^{208}Pb/^{204}Pb$ (±SD)	Eu* (±SD)	As/Al×1000	$(Mn/Al)_{UCC}$	$(Zn/Al)_{UCC}$	Zr/Nb	Zr/Hf	Zr/ΣREE
PSA_{LAM} (Libya-Algeria-Mali)	0.715 ± 0.003	−12.8 ± 1.8	18.65 ± 0.12	15.66 ± 0.04	38.93 ± 0.11	0.97 ± 0.08	0.9–3.4	0.4–1.3	1.0–1.5	4.1–6.5	34.4–37.5	0.5–0.6
PSA_{LE} (Libya-Egypt)	0.709 ± 0.003	−6.5 ± 3.7	18.53 ± 0.44	15.65 ± 0.05	38.45 ± 0.44	1.05 ± 0.08	1.1–2.5	0.7–1.3	1.1–9.1	5.1–10.5	35.7–39.8	0.7–1.3
PSA_{BD} (Bodélé Depression)	0.719 ± 0.004	−11.8 ± 1.8	19.07 ± 0.12	15.75 ± 0.03	39.46 ± 0.18	0.90 ± 0.02	0.3–0.8	0.8–1.2	1.0–1.2	4.6–5.9	36.6–38.5	0.4–0.6
PSA_{MC} (Mali Center)	0.730 ± 0.008	−16.8 ± 3.1	19.10 ± 0.01	15.76 ± 0.01	39.42 ± 0.03	1.02 ± 0.04	0.7	0.4	0.6–0.7	5.7	37.1–39.1	0.5–0.6
PSA_{WAC} (West African Coast)	0.724 ± 0.007	−12.9 ± 1.4	18.62 ± 0.17	15.67 ± 0.02	38.80 ± 0.16	1.05 ± 0.07	>1–20	0.4–1.6	0.8–2.3	5.7–8.1	31.7–39.1	0.4–0.7
PSA_{Ma} (Mauritania)	0.730 ± 0.007	−16.0 ± 1.5	n.d.	n.d.	n.d.	n.d.	n.d.	n.d.	n.d.	n.d.	n.d.	n.d.

regions and can thus be used as a dust provenance tracer with a relatively high degree of confidence.

In contrast with ε_{Nd}, higher $^{87}Sr/^{86}Sr$ are systematically found in the finer fractions (Fig. 2), in agreement with earlier studies (Dasch, 1969; Meyer et al., 2011). Even if the difference in $^{87}Sr/^{86}Sr$ between silt and clay fractions is relatively small compared to the regional variations in $^{87}Sr/^{86}Sr$ between North African soils (Scheuvens et al., 2013; references therein), the $^{87}Sr/^{86}Sr$ is shifted systematically towards more radiogenic signatures with increasing distance from the source due to winnowing which affects the grain size distribution. In addition to this grain size sorting, the effect of calcium carbonate dissolution is evident in the SC fraction which did not undergo acetic acid leaching in contrast to the other size fractions and which exhibits the lowest $^{87}Sr/^{86}Sr$ (Fig. 2). Based on the reported shift, calcium carbonate is the main carrier phase of Sr, and dissolution of this phase by sulfuric acid during atmospheric dust transport (Song and Carmichael, 1999) can significantly impact the $^{87}Sr/^{86}Sr$ signature found in the final dust deposit. This is particularly the case for samples collected in the PSA_{WAC} or PSA_{LE} where highly variable $CaCO_3$ contents are associated with a large range in $^{87}Sr/^{86}Sr$ ratios (see Table S5 and Fig. 5). Comparison between the <32 μm decarbonated fraction reported by Jewell et al. (2020) and the bulk fraction reported here for the same Bodélé samples provides firm evidence for a strong control of granulometry and mineralogy on Sr isotope fractionation (Fig. S1).

Whether or not Pb isotopes vary significantly with grain size, and thus are potentially altered relative to the source upon transport, remains unclear (Feng et al., 2010). Lead isotope ratios from the silty fractions are clearly distinct from those of other size fractions, but SC, C, and FC overlap within uncertainty (Fig. 2), irrespective of geographical region and local geology. This observation strongly suggests that the finer fractions ($\lesssim$2 μm) in the SC samples are the main carriers of Pb, which always tend to dominate the net isotope budget of deflated lithic materials in Saharan-Sahel dusts. Overall, the data at hand do not indicate that Pb isotopes are affected by grain-size sorting during long-range atmospheric transport.

However, the particle-reactive nature of Pb, especially that of anthropogenic origin, hampers the direct use of Pb isotope compositions of bulk continental materials in dust mineral provenance studies. Most of the isotope data available on modern aerosols/dust deposits have been obtained on the residual fraction left after removal of the more labile anthropogenic Pb using mild acid (~0.5 M HBr) (Bollhöfer et al., 1999; Kumar et al., 2014, 2018), With the exception of the four soil samples from Mali and Morocco (see section 3.1), this procedure was not adopted for the whole SC dataset since most of the soils analyzed were collected in places remote from human civilization. This is supported by the limited difference between the bulk SC fractions and the residues for Moroccan and Malian soils (Fig. S3) and by the observation that the vast majority of the Pb isotope data fall away from the known field of North African anthropogenic Pb (Fig. S9)(Bollhöfer and Rosman, 2000; Kumar et al., 2014). Likewise, virtually all soils have near-crustal $(Pb/Al)_{UCC}$ ratios – exceptions are two samples from the PSA_{LE} (SC-32 and SC-99), which exhibit elevated $(Pb/Al)_{UCC}$ ratios (Table S5) suggestive of some anthropogenic contribution. It should, however, be pointed out that the HBr leachates ("anthropogenic" component) display Pb isotope ratios, as well as $^{87}Sr/^{86}Sr$ and ε_{Nd}, which almost overlap those of lithic clays (Fig. S3), suggesting partial dissolution of the fine clays might occur during the HBr leaching step.

To summarize, while the radiogenic Sr isotope signature can help determine the origin/source of dust, the mineralogical, grain size, and regional signals cannot be unambiguously disentangled

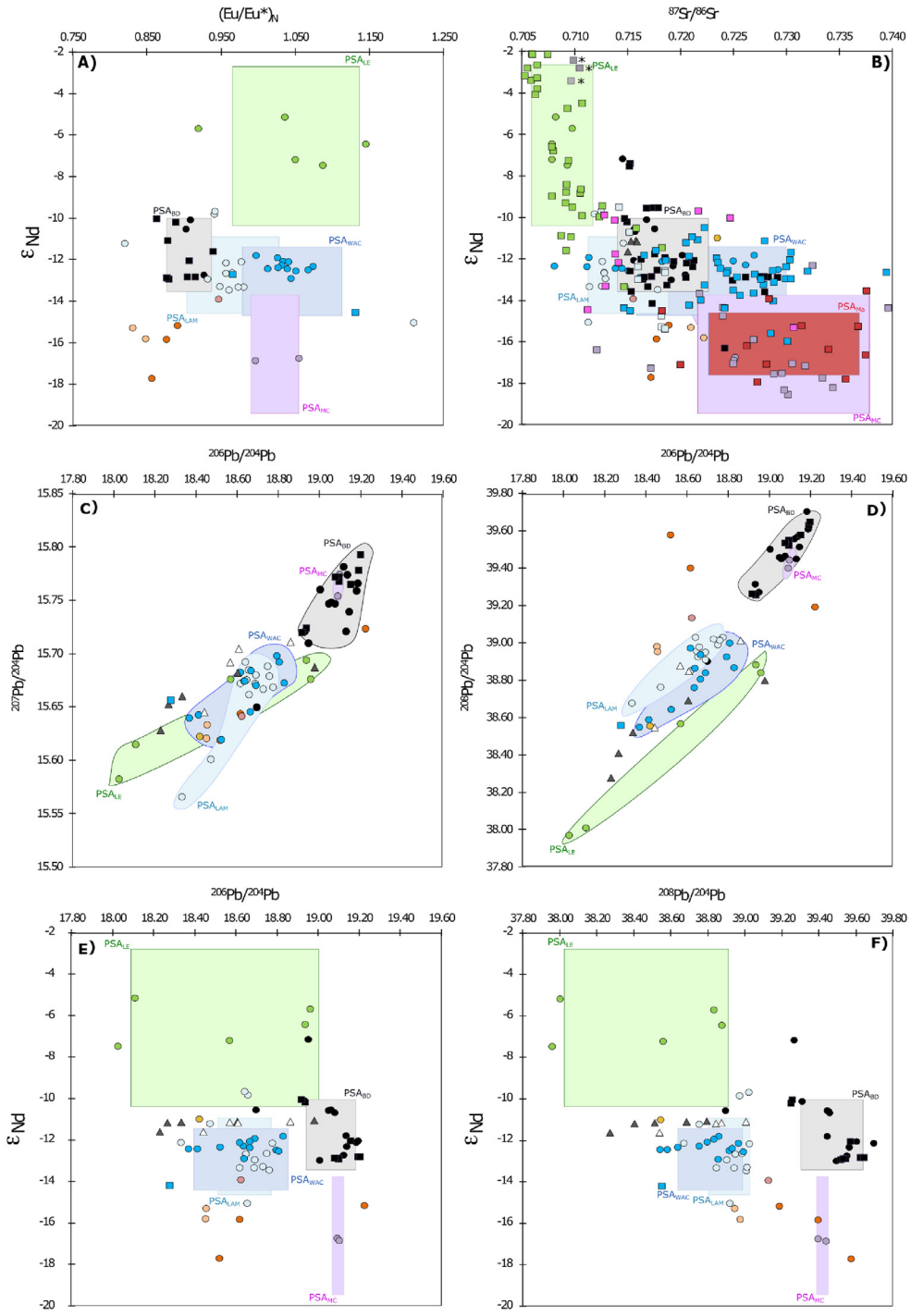
A)
B)
C)
D)
E)
F)
$(Eu/Eu^*)_N$
$^{87}Sr/^{86}Sr$
$^{206}Pb/^{204}Pb$
$^{207}Pb/^{204}Pb$
$^{208}Pb/^{204}Pb$
εNd
PSA_LE
PSA_BD
PSA_WAC
PSA_LAM
PSA_MC
PSA_Ma
Potential Source Areas
PSA_LE (Libya-Egypt) (this study)
PSA_LE (Libya-Egypt) (literature data ❶❷❸❹❿)
PSA_LAM (Libya-Algeria-Mali) (this study)
PSA_LAM (Libya-Algeria-Mali) (literature data ❸❹❺❿)
PSA_BD (Bodélé Depression) (this study)
PSA_BD (Bodélé Depression (literature data ❻❿)
PSA_MC (Mali Center) (this study)
PSA_MC (literature data ❶❷)
PSA_Ma (Mauritania) (literature data ❾❿)
Potential Source Areas
PSA_WAC (West African Coast) (this study)
PSA_WAC (West African Coast) (literature data ❶❷❼❽❾❿)
Non-representative dust sources
Unassigned SC-65 (this study)
Hoggar Mountains (this study)
Niger/Benin/Togo transect (literature data) ❷
Niger (this study)
Accessory data
Mali Soil ❽
Dust deposits along Harmattan Road bulk ❻
Dust deposits along Harmattan Road residue (this study)
❶ Gross et al. (2016)❷Zhao et al. (2018)❸Grousset and Biscaye (2005)❹Hamelin et al. (1990)❺Revel et al. (2010)
❻Abouchami et al. (2013)❼van der Does et al. (2018)❽Kumar et al. (2014)❾Grousset et al. (1998)❿ Grousset et al. (1992)⓫ Jewell et al. 2020.

from one another. The radiogenic Nd and Pb isotope systems, on the other hand, are more robust tracers of sources and regional origin of dusts.

6. Radiogenic isotope fingerprint of North African PSA

Long-lived radiogenic isotope systems (Rb–Sr, Sm–Nd, Th–U–Pb) vary among North African tectonic/stratigraphic units depending principally on geological basement age. This variability is reflected in the measured isotope compositions of the respective PSA of North African dusts. In the following discussion, we use the newly defined PSA subdivision based on REE patterns to constrain further their radiogenic isotope fingerprints. While our $^{87}Sr/^{86}Sr$ and ε_{Nd} data can be compared with existing literature data, our Pb isotope dataset is the first extensive one reported on North African soils, with the exception of the study by Abouchami et al. (2013) on the Bodélé Depression. All the radiogenic isotope data currently available are plotted in Fig. 5. Our reassessment of the spatial extent of the PSA is based on radiogenic isotope fingerprinting and the geographical extent of geological provinces (Ye et al., 2017). It is summarized in Fig. 6 where it is compared with the previously defined PSA of Formenti et al. (2011) as well as the most recent satellite-based dust source identification (Yu et al., 2018).

The PSA_{MC}, Hoggar Mountains and Niger soil samples exhibit unradiogenic ε_{Nd} (from −17.8 to −14.0) and radiogenic $^{87}Sr/^{86}Sr$ (0.715–0.725), consistent with soils developed on old African cratons. As mentioned in section 4, samples derived from the Hoggar and Niger regions can hardly be considered as a potential source area for dust due to the limited dust activity (Fig. 1) and the restricted area of sediment deposits originating from the Hoggar and Aïr Moutains (i.e. restricted to the Iullemmeden Basin, Ye et al., 2017). The radiogenic Sr–Nd isotope signatures from the Malian PSA_{MC} agree with previous measurements performed on soil and aerosols collected in the region (Kumar et al., 2014; Zhao et al., 2018), consistent with their development on Neoproterozoic to Cambrian terrains (1000-485 Ma, Fig. 1C). Emission of dust from soils in this region could potentially be identified based on its geologically "old" Sr-Nd-Pb isotope signature. However, since the PSA_{MC} is located south of satellite-imaged sites of dust activation seen in Fig. 6, this region can plausibly be only a very minor source of dust emission. In addition, radiogenic $^{87}Sr/^{86}Sr$ (above 0.725) and unradiogenic ε_{Nd} (below −14) signatures were also found in a limited area located in Mauritania (Fig. 5B). This "old" signature is associated with the northern extent of the Mauritanides and the Reguibat Shield which have both an Archean to Paleoproterozoic origin (Ye et al., 2017). So, based on the distinct Sr–Nd isotope signatures we observe in Fig. 5B between Mauritanian soil samples and the rest of the West African Coast region, we feel confident to classify Mauritania PSA_{Ma} as a single, unique source region.

The PSA_{WAC} (excluding Mauritania), PSA_{LAM} and PSA_{BD} do not exhibit a geologically "old" radiogenic Sr-Nd-Pb isotope composition. Instead, they all share a typical Saharan/Sahelian signature with ε_{Nd} lying between −14 and −11 and $^{87}Sr/^{86}Sr$ in the 0.713–0.732 range. These isotope compositions are consistent with literature data for decarbonated phases of aerosols, deposited dusts, or bulk and fine fractions of soils and sandstones reported from these areas (Abouchami and Zabel, 2003; Gross et al., 2016; Jewell et al., 2020; Kumar et al., 2014; Scheuvens et al., 2013 and references therein; van der Does et al., 2018; Zhao et al., 2018). The $^{87}Sr/^{86}Sr$ varies considerably from sample to sample, most likely a function of carbonate content. Nonetheless, the Nd isotope compositions are relatively homogeneous because Nd is mostly carried by non-carbonate detrital phases like clays. Based on the review of Ye et al. (2017) of the geological units in North Africa, it has been possible to delineate the geographical extent of these three main sources.

The Libya-Algeria-Mali PSA_{LAM} is mostly associated with preserved continental sediment deposited during the existence of the Saharan basin between the Early and Late Cretaceous (140-97 Ma). Preserved marine sediments formed during trans-Saharan seaway episodes (97-56 Ma) are only restricted to a small area located west of the Hoggar Moutains. This PSA_{LAM} extends from the south of the Hoggar and Aïr Mountains to the north of Algeria-Tunisia, and from the Taoudeni Basin at the west to the Murzuq Basin at the east (Fig. 6). For this PSA_{LAM}, the similarity in geochemical and isotope compositions observed over the whole region, as well as satellite-derived dust sources (Yu et al., 2018), shows that the previous division into two separate potential source areas – PSA1 and PSA3 – by Formenti et al. (2011) is probably not necessary. Indeed, an overlap was observed previously for tracers such as illite/kaolinite (I/K ratio) or carbonate content over the entire region (Formenti et al., 2011; Scheuvens et al., 2013). Based upon Fig. 6, the most active sources of the PSA_{LAM} are located near its southwest, southeast and northern boundaries.

The West African Coast PSA_{WAC}, now excluding Mauritanian PSA_{Ma}, is mostly developed on terrestrial sediments of Cretaceous, Paleogene, and Oligocene ages (Ye et al., 2017), explaining its close match with the Sr-Nd-Pb isotope signatures of the PSA_{LAM}. The northern and southern parts of the PSA_{WAC}, taken together, agree well with PSA2 defined by Formenti et al. (2011). However, satellite imagery indicates that, except for its central part, little dust is emitted from this region in comparison with the eastern part of the PSA_{LAM} (El Djouf Desert, Fig. 6). Based on their similar geological history, distinguishing between PSA_{WAC} and PSA_{LAM} dust origin is thus complex using radiogenic isotope compositions. However, PSA_{WAC} samples exhibit slightly more positive Eu anomalies even if the difference is not statistically significant (1.07–1.13 versus 0.88–1.05), as well as arsenic enrichment (see Fig. S8B), two potential tracers to differentiate them from PSA_{LAM} soils. Thus, while differences are subtle, combining geochemical fingerprinting with back-trajectory analysis is essential, as has been shown in previous studies (Kumar et al., 2018; Skonieczny et al., 2013).

Finally, the Bodélé Depression has been receiving a lot of attention for the past 15 years, as it is considered the dustiest place on Earth. Even though the whole Chad Basin is the result of an episode of sediment accumulation during the Neogene (Ye et al., 2017), a diversity of sedimentary units has been reported ranging from quartz-rich eolian sands to diatomites deposited as "Lake Megachad" dried up (Bristow et al., 2009). Even if dust lofting mixes these components up, three endmembers – "Fe-rich", "Si-rich" and "Ca-rich" – were identified on the basis of their distinct chemical and isotope compositions (Abouchami et al., 2013). The "Ca-rich" end member was found to have less radiogenic Pb and a more radiogenic Nd isotope signature than the other two endmembers. Additional sampling performed in the Chad region, from the eastern paleoriver system to the Bahr el Gazel watershed (Jewell et al., 2020), confirms the great variability in ε_{Nd} (−14.2 to −7.4) and $^{87}Sr/^{86}Sr$ (0.709–0.728), which becomes even larger if the Angamma Delta sediments (CH34 and CH39 in Table S1) are included (ε_{Nd} between −3.4 and −2.4). The newly analyzed samples

Fig. 5. Identification of PSA using radiogenic isotope proxies (Sr, Nd, Pb) and Eu anomalies. The dataset obtained for the fine fraction of soils in this study and the available literature data are reported in each subplot. In A), B), E) and F), PSA areas are delimited using the standard deviation (Table 1) of the whole ε_{Nd}, Eu*, $^{206}Pb/^{204}Pb$ and $^{208}Pb/^{204}Pb$ range (this study and literature data). In C) and D), the Pb isotope systematic of each PSA is delimited by hand-drawn fields.

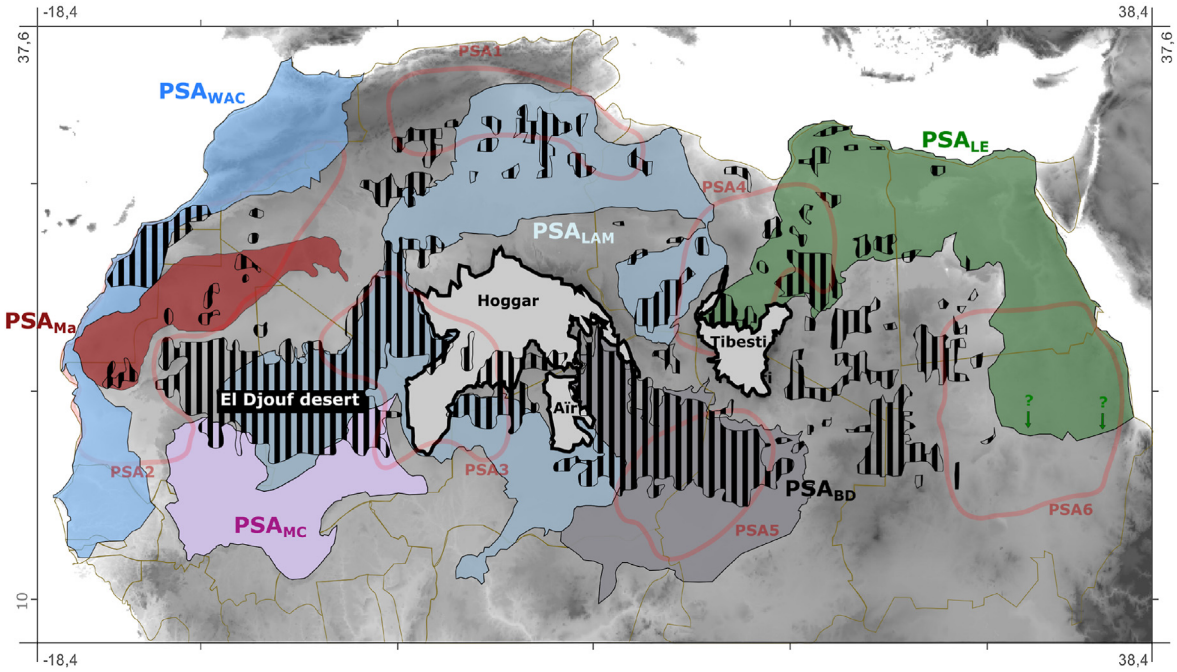

Fig. 6. Comparison of the newly-defined PSA with previous literature PSA (Formenti et al., 2011) and satellite-derived dust sources (Yu et al., 2018). The six PSA proposed by Formenti et al. (2011) on the basis of satellite observations are reported as thick light red ellipses. The black shaded areas correspond to dust sources based on dust plume motion averaged over 16 years (2000–2016) and detected using the MISR instrument on the Terra satellite (Yu et al., 2018). The six colored areas correspond to the newly defined PSA based on the extension of geological provinces summarized in Ye et al. (2017) and on the geochemical approach (Sr, Nd, Pb isotopes and REE patterns) presented in this study (Fig. 5), and include literature data for Mauritanian PSA (Grousset et al., 1998).

here combined with literature data show that the PSA_{BD} stands out clearly with respect to the other PSA, having the most radiogenic Pb signatures and negative Eu anomalies (Fig. 5). This radiogenic Pb signature is found in bulk and SC fractions (CH and SC samples, respectively, Table S1) and for sediments of distinct lithologies and sources, including in the Angamma Delta sediments (Table S1), underscoring the utility of Pb isotopes in dust source fingerprinting. The areal extent of the PSA_{BD} and associated eastern Chad Basin is in close agreement with the PSA5 originally defined by Formenti et al. (2011) – see Fig. 6. This region is considered to be one of the two main sources of North African dust (Yu et al., 2018). Even though its chemical signature is mostly defined by samples closely surrounding the Bodélé Depression, we can reasonably assume this to be representative of the whole Chad Basin region.

To conclude, the Libyan-Egyptian PSA_{LE} is characterized by radiogenic Nd (ε_{Nd} ranging from −12 to −3) and unradiogenic $^{87}Sr/^{86}Sr$ (0.706–0.713), typical of soils from regions containing juvenile volcanic rocks (Fig. 5). The extent of dust activity in the PSA_{LE} is still a matter of debate – Yu et al. (2018) suggested weak dust activity based upon dust motion analysis – whereas significant dust activation has been observed using MSG SEVIRI imagery, especially in the Nile River basin area (Bakker et al., 2019; Schepanski et al., 2009b). The extent of PSA_{LE} covers both PSA4 and the northern part of PSA6 suggesting that the distinction between these two regions by Formenti et al. (2011) is probably not necessary anymore (Fig. 6). Extension of the PSA_{LE} southwards toward northern Sudan is plausible, based on similar ε_{Nd} and $^{87}Sr/^{86}Sr$ with those of Nubian Desert alluvial sediments (Jewell et al., 2020). This inference is supported by Sr and Nd isotope compositions of Nile River sediments, which are inherited from drainage of Proterozoic basement and Cenozoic volcanic provinces (ε_{Nd} −7.5 to +3.4 and $^{87}Sr/^{86}Sr$ 0.704 to 0.715, Padoan et al., 2011). Thus, East African sources lying in the southern part of PSA6 are probably similar to those of our PSA_{LE}.

Based on Fig. 6 and the recent study of Bakker et al. (2019), the North Chad-North Sudan region – located southeastward of PSA_{LE} and eastwards of the PSA_{BD} – is a very active dust emission region that has largely been underestimated in the overall North African dust budget. Developed mostly on Mesozoic continental sediments, its geochemical characterization is presently not possible due to a lack of sample materials but is mandatory to complement our identification of the main North African dust PSA.

In summary, the three radiogenic isotope tracers (Sr, Nd and Pb), in combination with REE patterns and elemental compositions, enable us to provide an updated and clear-cut geographic subdivision of North African PSA dust emissions, each having a unique geochemical fingerprint. This geochemical characterization is summarized in Table 1.

7. Implications for the identification of modern and past dust sources

7.1. Fingerprinting the modern dust outflow

Dust outflow from North Africa follows a predominantly westward route with a large spatio-temporal dispersion over the Atlantic Ocean (Kaufman et al., 2005; Prospero and Carlson, 1972; Prospero et al., 1981; Swap et al., 1992). However, the relative dust contributions from sub-regions of North Africa (i.e. described in terms of PSA) have not proven to be possible. Modeling and satellite observations over the past fifteen years have suggested major dust contributions originating in the Bodélé Depression (PSA_{BD} = PSA5) in the boreal winter season, shifting to mostly PSA_{WAC} (former PSA2) and PSA_{LAM} (former PSA1 and PSA3) sources during the summer months (Ben-Ami et al., 2012; Engelstaedter and Washington, 2007; Koren et al., 2006). Recent studies relying on radiogenic isotopes as tracers of dust provenance have provided new insights into the sources and transport mode of dust across the

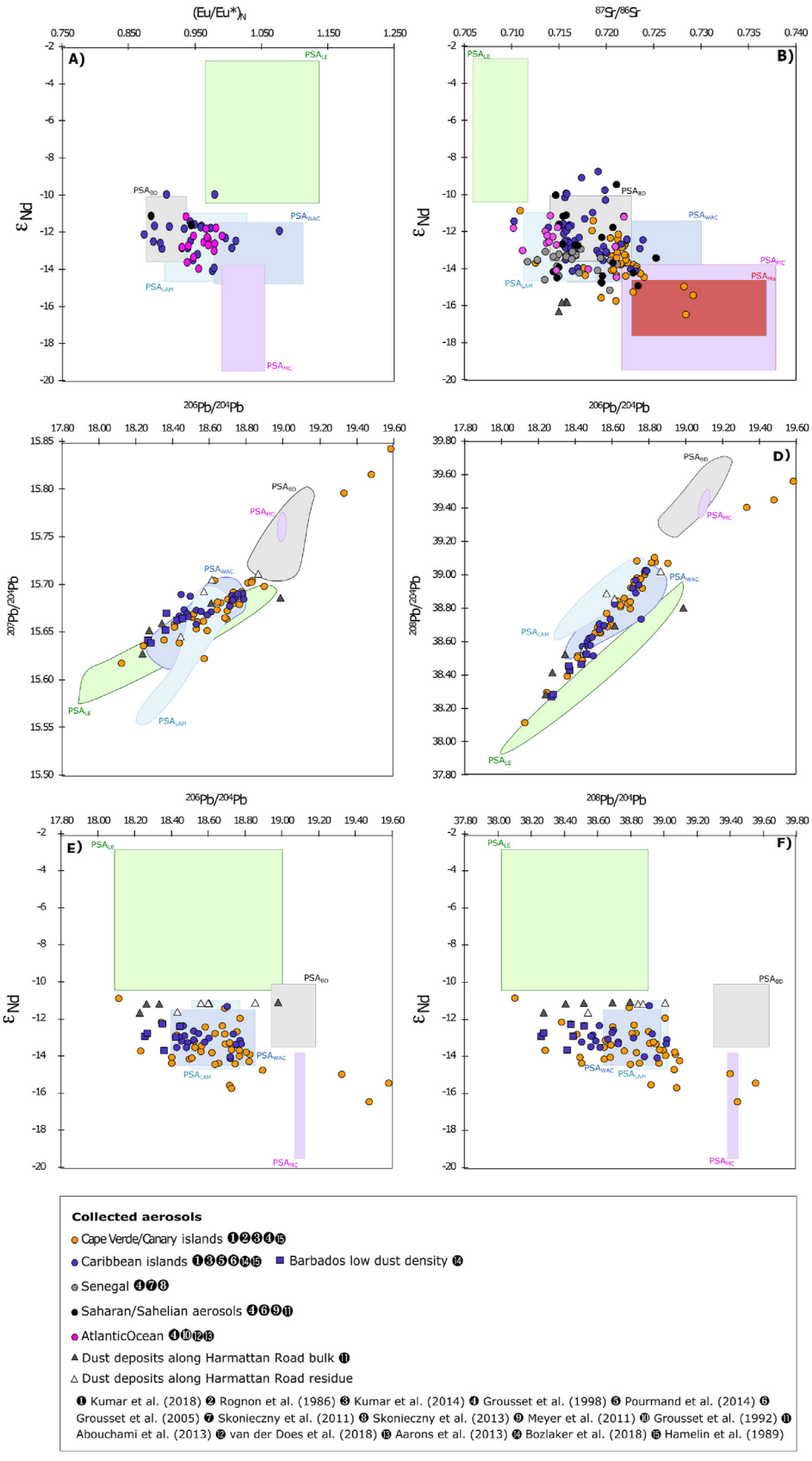

Fig. 7. Identification of the North African provenance of collected transatlantic dust samples based upon our newly defined PSA (see Fig. 5), shown as fields. The dataset is from the literature as listed in the legend.

Atlantic Ocean. Dust reaching the Cape Verde Islands and Barbados in the Caribbean throughout the year has a predominantly western Saharan-Sahelian isotope signature (Bozlaker et al., 2018; Kumar et al., 2018; Pourmand et al., 2014). However, the significance of Bodélé-derived dust (PSA_{BD}) for wintertime outflow towards the Equatorial and South Atlantic still remains very uncertain. Based on the new constraints brought by our updated dataset to characterize North African PSA, especially in the central Saharan-Sahelian region, we re-evaluate below the available literature data and reassess their importance and contribution to the overall dust budget over the Atlantic.

In order to pinpoint the PSA from which any dust originated, both the Eu anomalies and radiogenic Sr, Nd and Pb isotope signatures (Fig. 5) of the dust sample are used as discriminant criteria for each North African PSA we identified. The radiogenic isotope compositions of dusts collected over different locations in the Atlantic Ocean are reported in Table S4 and plotted in Fig. 7, with the delimited areas of North African PSA defined as in Fig. 5. The dust transport mechanisms differ between the eastern (low altitude transport to Cape Verde or Senegal, mainly during boreal winter) and western sides (high altitude transport towards the Caribbean, mainly during the summer) of the Atlantic Ocean (Schepanski et al., 2009a). However, the signature recorded in dust collected on both sides of the Atlantic is not strongly different between seasons or the year of sampling. The Eu/Eu*-ε_{Nd} and $^{87}Sr/^{86}Sr$-ε_{Nd} diagrams (Fig. 7A/B) demonstrate a predominance of Saharan-Sahelian sources (PSA_{BD}, PSA_{WAC} and PSA_{LAM}) for cross-Atlantic dust transport, with minimal contribution from PSA_{LE} or PSA from "older" geological provinces (PSA_{MC} or PSA_{Ma}). The exception proving the rule is the massive February 2012 outbreak event recorded at the Cape Verde Islands, which, as shown by Kumar et al. (2018), was at its peak typical of the Mauritanian PSA_{Ma} ($\varepsilon_{Nd} < -15$ and $^{87}Sr/^{86}Sr > 0.726$), suggesting that this source might be of importance for proximal dust transport.

In Pb isotope space, most of the dust samples also plot close to the Saharan-Sahelian PSA fields (Fig. 7C/D). The dispersion of Pb isotope signatures may result from either intra-PSA variability, as observed for PSA_{WAC} and PSA_{LAM} sources, or due to mixing in of disparate sources, such as Bodélé (more radiogenic) and anthropogenic Pb (less radiogenic). The first possibility seems more likely as anthropogenic Pb is usually removed from dust filters by prewashing with dilute HBr (Hamelin et al., 1989; Kumar et al., 2018). A similar chemical pre-treatment was applied to dust deposits collected along the Harmattan corridor in the Sahel (see Table S4), whose Pb isotope compositions may have been affected by anthropogenic Pb contamination (Abouchami et al., 2013). Here, a systematic shift towards more radiogenic Pb values is observed for the residues after the leaching treatment (triangles in Fig. 7C/D), confirming significant anthropogenic contamination of the lead in these samples. The anthropogenic-free signature is surprisingly not as radiogenic as would be expected for dust originating in the vicinity of the Bodélé Depression, which is especially true for the Faya-Largeau sample (Table S4). This observation suggests the existence of another dust source contributing to dust deposition in this region: for example, the undocumented North Sudan-North Chad source seen in Fig. 6.

Similar anthropogenic overprinting is expected for Barbados aerosols collected and analyzed by Bozlaker et al. (2018) as these were not subjected to HBr pre-treatment. Kumar et al. (2018) have shown that during high dust activity, samples collected have similar Pb isotope compositions to those of HBr pre-leached dust, as well as crustal-like Pb concentrations. This suggests that during very high dust loading, anthropogenic contributions form a lower proportion of the total lead present. But during low dust activity, the association of Pb enrichment with unradiogenic $^{206}Pb/^{204}Pb$, $^{207}Pb/^{204}Pb$ and $^{208}Pb/^{204}Pb$ signatures (Fig. 7C/D) is indicative of local anthropogenic inputs in the Barbados dataset of Bozlaker et al. (2018). Therefore, it is important to remove or at least minimize anthropogenic Pb contribution if one is to identify correctly dust provenance using the natural (non-anthropogenic) isotope composition.

Comparison between recorded radiogenic signatures on both sides of the Atlantic Ocean and our new assessment of North African PSA corroborates the inferences of Kumar et al. (2018) that West African sources (PSA_{WAC} and PSA_{LAM}) are the primary source for the North African outflow and outbreaks. Distinguishing between PSA_{WAC} and PSA_{LAM} sources is not totally straightforward as Eu anomalies (Fig. 5A) and As enrichments (Fig. S8B) are the only criteria differing between these two PSA. As was previously shown by Kumar et al. (2018), back-trajectory analysis is complementary and worthwhile to strengthen and confirm the geochemically based tracing of dust back to its source.

Regarding the PSA_{BD}, the apparent absence of long-range transport of Bodélé dust across the North Atlantic (especially in the Caribbean and southeastern USA) in summer, but also in the winter season (Schepanski et al., 2009a) is puzzling, as discussed by Kumar et al. (2018). However, the high deposition rate of aerosols (wet and dry) along the southwestward outbound trajectory (Harmattan corridor, Gläser et al., 2015; Yu et al., 2020), as well as the lack of an efficient mechanism to loft the dust to high altitude for long-range transport might provide an explanation. Several modelling studies suggest that the flow of Bodélé dust towards South America during the winter season is expected to dominate over other sources (Ben-Ami et al., 2010; Schepanski et al., 2009a), but the amount of Bodélé dust that completes the journey is questionable (Gläser et al., 2015; Prospero et al., 2020). The Sr and Nd isotope compositions of dust filters collected in French Guyana suggest that PSA_{LAM} and PSA_{BD} were the two major sources, with some interannual variability (Barkley et al., 2022). However, the sorting and mineralogical effect on $^{87}Sr/^{86}Sr$ discussed above can potentially affect these conclusions. Future analysis of dust samples collected from South America would benefit from Pb isotope data which have been shown to be diagnostic of Bodélé Depression material and potentially can add constraints on the dust provenance.

7.2. Application to Quaternary archives

Our data could also be valuable for identifying dust origin and wind patterns in paleo-dust records using marine and terrestrial archives. Changes of dust provenance during glacial/interglacial cycles have been documented at a global scale (Mahowald et al., 2011; McGee et al., 2010). However, characterizing the worldwide dust sources using different proxies, as it is done in this study for the North Africa region, is mandatory to refine dust provenance and identify feedbacks between atmospheric dust and climate changes (Újvári et al., 2022). At the regional scale, Gili et al. (2017) determined and used Sr-Nd-REE signatures of South American dust sources to identify the dust provenance and the associated wind reconstruction recorded in Southern Ocean sediment cores. North Africa experienced also large climatic and environmental variations during glacial-interglacial cycles, African Humid Periods and Henrich events (e.g. Claussen et al., 2017). Larger dust fluxes were recorded in sediment cores off Africa during glacial periods and associated with orbital forcings lowering precipitation intensity and vegetation cover extension (Zabel et al., 2001). However, using an improved methodology, recent African dust fluxes calculated over 240 ka from a West African margin sediment core question the correlation between dust flux and glacial/interglacial periods and instead attributed dust outflow variations to summer insolation

cycles (Skonieczny et al., 2019). Based on our updated PSA fingerprinting, it should be interesting to see if radiogenic isotope signatures can help distinguishing between these scenarios. At a millennial scale, the onsets of African Humid Periods or the effect of Heinrich events on North African paleoenvironments are, at least partially, decoupled from orbital considerations (Claussen et al., 2017). Heinrich events are coinciding with the southward shift of the Sahara-Sahel boundary and the strengthening of dust export (Collins et al., 2013; Mulitza et al., 2008). However, the respective strengthening of Northeast Trade Winds (NTW) from Algeria to the Mauritanian coast and of African Easterly Jets (AEJ) is not fully constrained yet. Since, both systems will preferentially mobilize different PSA (mostly PSA_{WAC} and PSA_{LAM} for NTW and PSA_{BD} for AEJ, respectively), Pb isotopes, the best tracer of Bodélé origin, may be used in association with Sr–Nd isotope compositions, for which subtle variations are difficult to interpret alone (Meyer et al., 2011). Finally, the occurrence of irregular African Humid Periods with time (5–10, 90–100 and 130–140 ka BP) has been extensively documented in the literature (Claussen et al., 2017 and references therein). Insolation maxima and the northward penetration of the monsoonal system increased the precipitation during the dry season and lowered precipitation seasonality, resulting in a green vegetated Sahara covered with megalakes (Tierney et al., 2011). However, understanding the timing of the abrupt termination of this event is still a matter of debate due to the complex interplay evidenced at a regional scale (Claussen et al., 2017). In that sense, the use of our updated PSA dataset, and particularly of Pb isotopes, may help to identify a more accurate timing of megalake drying and thus of the central African region activation, including the Bodélé Depression, as a potentially effective dust supplier.

8. Conclusions

We present a new revised subdivision of North African dust potential source areas (PSA) based on a comprehensive coupled geochemical and isotope tracer approach. This incorporates rare-earth element (REE) patterns, radiogenic Sr-Nd-Pb isotope compositions, as well as selected elemental ratios. The isotope and chemical fingerprint of these six new PSA are summarized in Table 1. In association with satellite observations and back-trajectory analysis, these PSA can serve as key tools for reconstructing North African dust fluxes, origin, and transport in the modern Earth System.

By combining Pb isotopes ratios, REE patterns, and selected elemental ratios, far more definitive and reliable constraints can be placed on the activation or deactivation of different North African PSA over time. Such constraints on dust provenance, as well as dust flux, provide invaluable information on biogeochemical cycles, climate, and land surface evolution – including position and strength of the African monsoon, intensity of low-level jets, land use, and sediment supply.

Author credit statement

This study was conceived by WA and SJG. Samples were provided by KK and CB. SPS designed and performed granulometric/leaching experiments. The dataset was obtained by SPS (isotopes) and DG (elemental). Initial drafts and interpretation were by DG and SPS. All authors contributed to the discussion, synthesis, and refinement of contents, and approved the final version of the manuscript.

Declaration of competing interest

The authors declare that they have no known competing financial interests or personal relationships that could have appeared to influence the work reported in this paper.

Data availability

Data will be made available on request.

Acknowledgments

Many of the samples, on which this study is based, were taken from a desert soil collection ("Mainz Sandbank"), which was originally hosted at the Institute for Physics of the Atmosphere (IPA) of the University of Mainz, before it was transferred to the Technical University of Darmstadt. The Sandbank was initiated in the late 1960s by Ruprecht Jaenicke and cared for by Lothar Schütz for many years (both IPA). Numerous contributors provided samples from their scientific and non-scientific trips to regions, which are not easily accessible for various reasons. Their contributions are hereby thankfully acknowledged. Siegfried Herrmann, Reimund Jotter, and Heinz Feldmann are thanked for their technical assistance during the acquisition of the chemical and isotope analyses. Lastly, we thank the editor Giovanni Zanchetta as well as the anonymous reviewers for their thoughts and insight. KK was funded by the Deutsche Forschungsgemeinschaft (DFG), grants 264907654 and 416816480. WA was funded by the DFG SPP1833 "Building a Habitable Earth". SPS was partly funded by Science and Engineering Research Board (SERB)-DST, India (CRG/2019/001141). This study was supported by the German Max Planck Society.

Appendix A. Supplementary data

Supplementary data to this article can be found online at https://doi.org/10.1016/j.quascirev.2022.107729.

References

Aarons, S.M., Aciego, S.M., Gleason, J.D., 2013. Variable Hf, Sr, Nd radiogenic isotopic compositions in a Saharan dust storm over the Atlantic: implications for dust flux to oceans, ice sheets and the terrestrial biosphere. Chem. Geol. 349–350, 18–26.

Abouchami, W., Näthe, K., Kumar, A., Galer, S.J.G., Jochum, K.P., Williams, E., Horbe, A.M.C., Rosa, J.W.C., Balsam, W., Adams, D., Mezger, K., Andreae, M.O., 2013. Geochemical and isotopic characterization of the Bodélé Depression dust source and implications for transatlantic dust transport to the Amazon Basin. Earth Planet Sci. Lett. 380, 112–123.

Abouchami, W., Zabel, M., 2003. Climate forcing of the Pb isotope record of terrigenous input into the Equatorial Atlantic. Earth Planet Sci. Lett. 213, 221–234.

Ansmann, A., Rittmeister, F., Engelmann, R., Basart, S., Jorba, O., Spyrou, C., Remy, S., Skupin, A., Baars, H., Seifert, P., Senf, F., Kanitz, T., 2017. Profiling of Saharan dust from the Caribbean to western Africa – Part 2: shipborne lidar measurements versus forecasts. Atmos. Chem. Phys. 17, 14987–15006.

Ashpole, I., Washington, R., 2012. An automated dust detection using SEVIRI: a multiyear climatology of summertime dustiness in the central and Western Sahara. J. Geophys. Res. Atmos. 117, D08202.

Ashpole, I., Washington, R., 2013a. Intraseasonal variability and atmospheric controls on daily dust occurrence frequency over the central and Western Sahara during the boreal summer. J. Geophys. Res. Atmos. 118, 12915–12926.

Ashpole, I., Washington, R., 2013b. A new high-resolution central and western Saharan summertime dust source map from automated satellite dust plume tracking. J. Geophys. Res. Atmos. 118, 6981–6995.

Bakker, N.L., Drake, N.A., Bristow, C.S., 2019. Evaluating the relative importance of northern African mineral dust sources using remote sensing. Atmos. Chem. Phys. 19, 10525–10535.

Barkley, A.E., Pourmand, A., Longman, J., Sharifi, A., Prospero, J.M., Panechou, K., Bakker, N., Drake, N., Guinoiseau, D., Gaston, C.J., 2022. Interannual variability in the source location of North African dust transported to the Amazon. Geophys. Res. Lett., e2021GL097344

Barkley, A.E., Prospero, J.M., Mahowald, N., Hamilton, D.S., Popendorf, K.J., Oehlert, A.M., Pourmand, A., Gatineau, A., Panechou-Pulcherie, K., Blackwelder, P., Gaston, C.J., 2019. African biomass burning is a substantial source of phosphorus deposition to the Amazon, Tropical Atlantic Ocean, and Southern Ocean. Proc. Natl. Acad. Sci. USA 116, 16216–16221.

Ben-Ami, Y., Koren, I., Altaratz, O., Kostinski, A., Lehahn, Y., 2012. Discernible rhythm

in the spatio/temporal distributions of transatlantic dust. Atmos. Chem. Phys. 12, 2253–2262.
Ben-Ami, Y., Koren, I., Rudich, Y., Artaxo, P., Martin, S.T., Andreae, M.O., 2010. Transport of North african dust from the Bodélé depression to the amazon basin: a case study. Atmos. Chem. Phys. 10, 7533–7544.
Bollhöfer, A., Chisholm, W., Rosman, K.J.R., 1999. Sampling aerosols for lead isotopes on a global scale. Anal. Chim. Acta 390, 227–235.
Bollhöfer, A., Rosman, K.J.R., 2000. Isotopic source signatures for atmospheric lead: the Southern Hemisphere. Geochem. Cosmochim. Acta 64, 3251–3262.
Bozlaker, A., Prospero, J.M., Price, J., Chellam, S., 2018. Linking Barbados mineral dust aerosols to North African sources using elemental composition and radiogenic Sr, Nd, and Pb isotope signatures. J. Geophys. Res. Atmos. 123, 1384–1400.
Bristow, C.S., Drake, N., Armitage, S., 2009. Deflation in the dustiest place on earth: the Bodélé depression, Chad. Geomorphology 105, 50–58.
Bristow, C.S., Moller, T.H., 2018. Testing the auto-abrasion hypothesis for dust production using diatomite dune sediments from the Bodélé Depression in Chad. Sedimentology 65, 1322–1330.
Chen, J., Li, G., Yang, J., Rao, W., Lu, H., Balsam, W., Sun, Y., Ji, J., 2007. Nd and Sr isotopic characteristics of Chinese deserts: implications for the provenances of Asian dust. Geochem. Cosmochim. Acta 71, 3904–3914.
Claussen, M., Dallmeyer, A., Bader, J., 2017. Theory and modeling of the African humid period and the green Sahara. In: Oxford Research Encyclopedia of Climate Science.
Collins, J.A., Govin, A., Mulitza, S., Heslop, D., Zabel, M., Hartmann, J., Röhl, U., Wefer, G., 2013. Abrupt shifts of the sahara–sahel boundary during Heinrich stadials. Clim. Past 9, 1181–1191.
Dasch, E.J., 1969. Strontium isotopes in weathering profiles, deep-sea sediments, and sedimentary rocks. Geochem. Cosmochim. Acta 33, 1521–1552.
Dessert, C., Clergue, C., Rousteau, A., Crispi, O., Benedetti, M.F., 2020. Atmospheric contribution to cations cycling in highly weathered catchment, Guadeloupe (Lesser Antilles). Chem. Geol. 531, 119354.
Engelstaedter, S., Washington, R., 2007. Atmospheric controls on the annual cycle of North African dust. J. Geophys. Res. Atmos. 112, D03103.
Feng, J.-L., Hu, Z.-G., Cui, J.-Y., Zhu, L.-P., 2010. Distributions of lead isotopes with grain size in aeolian deposits. Terra. Nova 22, 257–263.
Ferrat, M., Weiss, D.J., Strekopytov, S., Dong, S., Chen, H., Najorka, J., Sun, Y., Gupta, S., Tada, R., Sinha, R., 2011. Improved provenance tracing of Asian dust sources using rare earth elements and selected trace elements for palaeomonsoon studies on the eastern Tibetan Plateau. Geochem. Cosmochim. Acta 75, 6374–6399.
Formenti, P., Caquineau, S., Desboeufs, K., Klaver, A., Chevaillier, S., Journet, E., Rajot, J.L., 2014. Mapping the physico-chemical properties of mineral dust in western Africa: mineralogical composition. Atmos. Chem. Phys. 14, 10663–10686.
Formenti, P., Schütz, L., Balkanski, Y., Desboeufs, K., Ebert, M., Kandler, K., Petzold, A., Scheuvens, D., Weinbruch, S., Zhang, D., 2011. Recent progress in understanding physical and chemical properties of African and Asian mineral dust. Atmos. Chem. Phys. 11, 8231–8256.
Galer, S.J.G., 1999. Optimal double and triple spiking for high precision lead isotopic measurement. Chem. Geol. 157, 255–274.
Gee, G.W., Or, D., 2002. Particle-size analysis. In: Dane, J.H., Topp, G.C. (Eds.), Methods of Soil Analysis. Part 4. Physical Methods. Soil Science Society of America, Inc., Madison, Wisconsin, USA.
Giles, J., 2005. The dustiest place on Earth. Nature 434, 816–819.
Gili, S., Gaiero, D.M., Goldstein, S.L., Chemale, F., Jweda, J., Kaplan, M.R., Becchio, R.A., Koester, E., 2017. Glacial/interglacial changes of Southern Hemisphere wind circulation from the geochemistry of South American dust. Earth Planet Sci. Lett. 469, 98–109.
Ginoux, P., Prospero, J.M., Gill, T.E., Hsu, N.C., Zhao, M., 2012. Global-scale attribution of anthropogenic and natural dust sources and their emission rates based on MODIS Deep Blue aerosol products. Rev. Geophys. 50, RG3005.
Gläser, G., Wernli, H., Kerkweg, A., Teubler, F., 2015. The transatlantic dust transport from North Africa to the Americas—its characteristics and source regions. J. Geophys. Res. Atmos. 120 (11), 231-211,252.
Goudie, A.S., Middleton, N.J., 2006. Desert Dust in the Global System. Springer Science & Business Media.
Gross, A., Palchan, D., Krom, M.D., Angert, A., 2016. Elemental and isotopic composition of surface soils from key Saharan dust sources. Chem. Geol. 442, 54–61.
Grousset, F.E., Biscaye, P.E., 2005. Tracing dust sources and transport patterns using Sr, Nd and Pb isotopes. Chem. Geol. 222, 149–167.
Grousset, F.E., Parra, M., Bory, A., Martinez, P., Bertrand, P., Shimmield, G., Ellam, R.M., 1998. Saharan wind regimes traced by the Sr-Nd isotopic composition of subtropical Atlantic sediments: last glacial maximum vs. today. Quat. Sci. Rev. 17, 395–409.
Grousset, F.E., Rognon, P., Coudé-Gaussen, G., Pédemay, P., 1992. Origins of peri-Saharan dust deposits traced by their Nd and Sr isotopic composition. Palaeogeogr. Palaeoclimatol. Palaeoecol. 93, 203–212.
Haarig, M., Walser, A., Ansmann, A., Dollner, M., Althausen, D., Sauer, D., Farrell, D., Weinzierl, B., 2019. Profiles of cloud condensation nuclei, dust mass concentration, and ice-nucleating-particle-relevant aerosol properties in the Saharan Air Layer over Barbados from polarization lidar and airborne in situ measurements. Atmos. Chem. Phys. 19, 13773–13788.
Hamelin, B., Grousset, F., Sholkovitz, E.R., 1990. Pb isotopes in surficial pelagic sediments from the North Atlantic. Geochem. Cosmochim. Acta 54, 37–47.
Hamelin, B., Grousset, F.E., Biscaye, P.E., Zindler, A., Prospero, J.M., 1989. Lead isotopes in trade-wind aerosols at Barbados - the influence of European emissions over the North Atlantic. Journal of Geophysical Research-Oceans 94, 16243–16250.
Harlavan, Y., Erel, Y., 2002. The release of Pb and REE from granitoids by the dissolution of accessory phases. Geochem. Cosmochim. Acta 66, 837–848.
Hudson-Edwards, K.A., Bristow, C.S., Cibin, G., Mason, G., Peacock, C.L., 2014. Solid-phase phosphorus speciation in Saharan Bodélé Depression dusts and source sediments. Chem. Geol. 384, 16–26.
IUCN/PACO, 2012. Mining sector development in West Africa and its impact on conservation. In: IUCN/PACO. Burkina Faso, Gland, Switzerland and Ouagadougou.
Jewell, A.M., Drake, N., Crocker, A.J., Bakker, N.L., Kunkelova, T., Bristow, C.S., Cooper, M.J., Milton, J.A., Breeze, P.S., Wilson, P.A., 2020. Three North African dust source areas and their geochemical fingerprint. Earth Planet Sci. Lett., 116645
Jochum, K.P., Weis, U., Schwager, B., Stoll, B., Wilson, S.A., Haug, G.H., Andreae, M.O., Enzweiler, J., 2016. Reference values following ISO guidelines for frequently requested rock reference materials. Geostand. Geoanal. Res. 40, 333–350.
Jones, J.V.I., Piatak, N.M., Bedinger, G.M., 2017. Zirconium and hafnium. In: Schulz, K.J., DeYoung, J.J.H., Seal li, R.R., Bradley, D.C. (Eds.), Economic and Environmental Geology and Prospects for Future Supply: U.S. Geological Survey Professional Paper 1802, pp. V1–V26.
Kanayama, S., Yabuki, S., Zeng, F., Liu, M., Shen, Z., Liu, L., Yanagisawa, F., Abe, O., 2005. Size-dependent geochemical characteristics of Asian dust - Sr and Nd isotope compositions as tracers for source identification -. Journal of the Meteorological Society of Japan. Ser. II 83A, 107–120.
Kaufman, Y.J., Koren, I., Remer, L.A., Tanré, D., Ginoux, P., Fan, S., 2005. Dust transport and deposition observed from the terra-moderate resolution imaging spectroradiometer (MODIS) spacecraft over the Atlantic Ocean. J. Geophys. Res. Atmos. 110.
Klose, M., Shao, Y., Karremann, M.K., Fink, A.H., 2010. Sahel dust zone and synoptic background. Geophys. Res. Lett. 37, L09802.
Koren, I., Kaufman, Y.J., Washington, R., Todd, M.C., Rudich, Y., Martins, J.V., Rosenfeld, D., 2006. The Bodélé depression: a single spot in the Sahara that provides most of the mineral dust to the Amazon forest. Environ. Res. Lett. 1, 014005.
Kumar, A., Abouchami, W., Galer, S.J.G., Garrison, V.H., Williams, E., Andreae, M.O., 2014. A radiogenic isotope tracer study of transatlantic dust transport from Africa to the Caribbean. Atmos. Environ. 82, 130–143.
Kumar, A., Abouchami, W., Galer, S.J.G., Singh, S.P., Fomba, K.W., Prospero, J.M., Andreae, M.O., 2018. Seasonal radiogenic isotopic variability of the African dust outflow to the tropical Atlantic Ocean and across to the Caribbean. Earth Planet Sci. Lett. 487, 94–105.
Mahowald, N., Albani, S., Engelstaedter, S., Winckler, G., Goman, M., 2011. Model insight into glacial–interglacial paleodust records. Quat. Sci. Rev. 30, 832–854.
Mahowald, N.M., Baker, A.R., Bergametti, G., Brooks, N., Duce, R.A., Jickells, T.D., Kubilay, N., Prospero, J.M., Tegen, I., 2005. Atmospheric global dust cycle and iron inputs to the ocean. Global Biogeochem. Cycles 19.
McGee, D., Broecker, W.S., Winckler, G., 2010. Gustiness: the driver of glacial dustiness? Quat. Sci. Rev. 29, 2340–2350.
Meyer, I., Davies, G.R., Stuut, J.-B.W., 2011. Grain size control on Sr-Nd isotope provenance studies and impact on paleoclimate reconstructions: an example from deep-sea sediments offshore NW Africa. G-cubed 12, Q03005.
Moran-Zuloaga, D., Ditas, F., Walter, D., Saturno, J., Brito, J., Carbone, S., Chi, X., Hrabě de Angelis, I., Baars, H., Godoi, R.H.M., Heese, B., Holanda, B.A., Lavrič, J.V., Martin, S.T., Ming, J., Pöhlker, M.L., Ruckteschler, N., Su, H., Wang, Y., Wang, Q., Wang, Z., Weber, B., Wolff, S., Artaxo, P., Pöschl, U., Andreae, M.O., Pöhlker, C., 2018. Long-term study on coarse mode aerosols in the Amazon rain forest with the frequent intrusion of Saharan dust plumes. Atmos. Chem. Phys. 18, 10055–10088.
Moreno, T., Querol, X., Castillo, S., Alastuey, A., Cuevas, E., Herrmann, L., Mounkaila, M., Elvira, J., Gibbons, W., 2006. Geochemical variations in aeolian mineral particles from the sahara–sahel dust corridor. Chemosphere 65, 261–270.
Moskowitz, B.M., Reynolds, R.L., Goldstein, H.L., Berquó, T.S., Kokaly, R.F., Bristow, C.S., 2016. Iron oxide minerals in dust-source sediments from the Bodélé Depression, Chad: implications for radiative properties and Fe bioavailability of dust plumes from the Sahara. Aeolian Research 22, 93–106.
Muhs, D.R., Budahn, J.R., Prospero, J.M., Carey, S.N., 2007. Geochemical evidence for African dust inputs to soils of western Atlantic islands: Barbados, the Bahamas, and Florida. J. Geophys. Res.: Earth Surf. 112.
Mulitza, S., Prange, M., Stuut, J.B., Zabel, M., Von Dobeneck, T., Itambi, A.C., Nizou, J., Schulz, M., Wefer, G., 2008. Sahel megadroughts triggered by glacial slowdowns of Atlantic meridional overturning. Paleoceanography 23.
Nogueira, J., Evangelista, H., Valeriano, C.d.M., Sifeddine, A., Neto, C., Vaz, G., Moreira, L.S., Cordeiro, R.C., Turcq, B., Aniceto, K.C., Neto, A.B., Martins, G., Barbosa, C.G.G., Godoi, R.H.M., Shimizu, M.H., 2021. Dust arriving in the Amazon basin over the past 7,500 years came from diverse sources. Communications Earth & Environment 2, 5.
Padoan, M., Garzanti, E., Harlavan, Y., Villa, I.M., 2011. Tracing Nile sediment sources by Sr and Nd isotope signatures (Uganda, Ethiopia, Sudan). Geochem. Cosmochim. Acta 75, 3627–3644.
Pourmand, A., Prospero, J.M., Sharifi, A., 2014. Geochemical fingerprinting of trans-

Atlantic African dust based on radiogenic Sr-Nd-Hf isotopes and rare earth element anomalies. Geology 42, 675–678.
Prospero, J.M., Barkley, A.E., Gaston, C.J., Gatineau, A., Campos y Sansano, A., Panechou, K., 2020. Characterizing and quantifying african dust transport and deposition to south America: implications for the phosphorus budget in the amazon basin. Global Biogeochem. Cycles 34, e2020GB006536.
Prospero, J.M., Carlson, T.N., 1972. Vertical and areal distribution of Saharan dust over the western equatorial north Atlantic Ocean. J. Geophys. Res. 77, 5255–5265, 1896-1977.
Prospero, J.M., Collard, F.-X., Molinié, J., Jeannot, A., 2014. Characterizing the annual cycle of African dust transport to the Caribbean Basin and South America and its impact on the environment and air quality. Global Biogeochem. Cycles 28, 757–773.
Prospero, J.M., Ginoux, P., Torres, O., Nicholson, S.E., Gill, T.E., 2002. Environmental characterization of global sources of atmospheric soil dust identified with the Nimbus 7 Total Ozone Mapping Spectrometer (TOMS) absorbing aerosol product. Rev. Geophys. 40, 2-1-2-31.
Prospero, J.M., Glaccum, R.A., Nees, R.T., 1981. Atmospheric transport of soil dust from Africa to South America. Nature 289, 570–572.
Prospero, J.M., Mayol-Bracero, O.L., 2013. Understanding the transport and impact of african dust on the caribbean basin. Bull. Am. Meteorol. Soc. 94, 1329–1337.
Reichholf, J.H., 1986. Is saharan dust a major source of nutrients for the amazonian rain forest? Stud. Neotrop. Fauna Environ. 21, 251–255.
Revel, M., Ducassou, E., Grousset, F.E., Bernasconi, S.M., Migeon, S., Revillon, S., Mascle, J., Murat, A., Zaragosi, S., Bosch, D., 2010. 100,000 Years of African monsoon variability recorded in sediments of the Nile margin. Quat. Sci. Rev. 29, 1342–1362.
Rittmeister, F., Ansmann, A., Engelmann, R., Skupin, A., Baars, H., Kanitz, T., Kinne, S., 2017. Profiling of Saharan dust from the Caribbean to western Africa – Part 1: layering structures and optical properties from shipborne polarization/Raman lidar observations. Atmos. Chem. Phys. 17, 12963–12983.
Rizzolo, J.A., Barbosa, C.G.G., Borillo, G.C., Godoi, A.F.L., Souza, R.A.F., Andreoli, R.V., Manzi, A.O., Sá, M.O., Alves, E.G., Pöhlker, C., Angelis, I.H., Ditas, F., Saturno, J., Moran-Zuloaga, D., Rizzo, L.V., Rosário, N.E., Pauliquevis, T., Santos, R.M.N., Yamamoto, C.I., Andreae, M.O., Artaxo, P., Taylor, P.E., Godoi, R.H.M., 2017. Soluble iron nutrients in Saharan dust over the central Amazon rainforest. Atmos. Chem. Phys. 17, 2673–2687.
Rognon, P., Coudé-Goussen, G., Revel, M., Grousset, F.E., P., P., 1996. Holocene Saharan dust deposition on the Cape Verde Islands: sedimentological and Nd-Sr isotopic evidence. Sedimentology 43, 359–366.
Rosner, B., 1983. Percentage points for a generalized ESD many-outlier procedure. Technometrics 25, 165–172.
Rudnick, R.L., Gao, S., 2014. 4.1 - composition of the continental crust A2. In: Holland, H.D., Turekian, K.K. (Eds.), Treatise on Geochemistry, second ed. Elsevier, Oxford, pp. 1–51.
Schepanski, K., Heinold, B., Tegen, I., 2017. Harmattan, Saharan heat low, and West African monsoon circulation: modulations on the Saharan dust outflow towards the North Atlantic. Atmos. Chem. Phys. 17, 10223–10243.
Schepanski, K., Tegen, I., Macke, A., 2009a. Saharan dust transport and deposition towards the tropical northern Atlantic. Atmos. Chem. Phys. 9, 1173–1189.
Schepanski, K., Tegen, I., Todd, M.C., Heinold, B., Bönisch, G., Laurent, B., Macke, A., 2009b. Meteorological processes forcing Saharan dust emission inferred from MSG-SEVIRI observations of subdaily dust source activation and numerical models. J. Geophys. Res. Atmos. 114, D10201.
Scheuvens, D., Schütz, L., Kandler, K., Ebert, M., Weinbruch, S., 2013. Bulk composition of northern African dust and its source sediments — a compilation. Earth Sci. Rev. 116, 170–194.
Shao, Y., Wyrwoll, K.-H., Chappell, A., Huang, J., Lin, Z., McTainsh, G.H., Mikami, M., Tanaka, T.Y., Wang, X., Yoon, S., 2011. Dust cycle: an emerging core theme in Earth system science. Aeolian Research 2, 181–204.
Skonieczny, C., Bory, A., Bout-Roumazeilles, V., Abouchami, W., Galer, S.J.G., Crosta, X., Diallo, A., Ndiaye, T., 2013. A three-year time series of mineral dust deposits on the West African margin: sedimentological and geochemical signatures and implications for interpretation of marine paleo-dust records. Earth Planet Sci. Lett. 364, 145–156.
Skonieczny, C., Bory, A., Bout-Roumazeilles, V., Abouchami, W., Galer, S.J.G., Crosta, X., Stuut, J.-B., Meyer, I., Chiapello, I., Podvin, T., Chatenet, B., Diallo, A., Ndiaye, T., 2011. The 7–13 March 2006 major Saharan outbreak: multiproxy characterization of mineral dust deposited on the West African margin. J. Geophys. Res. Atmos. 116, D18210.
Skonieczny, C., McGee, D., Winckler, G., Bory, A., Bradtmiller, L.I., Kinsley, C.W., Polissar, P.J., De Pol-Holz, R., Rossignol, L., Malaizé, B., 2019. Monsoon-driven Saharan dust variability over the past 240,000 years. Sci. Adv. 5, eaav1887.
Song, C.H., Carmichael, G.R., 1999. The aging process of naturally emitted aerosol (sea-salt and mineral aerosol) during long range transport. Atmos. Environ. 33, 2203–2218.
Swap, R., Garstang, M., Greco, S., Talbot, R., Kållberg, P., 1992. Saharan dust in the amazon basin. Tellus B 44, 133–149.
Tegen, I., 2003. Modeling the mineral dust aerosol cycle in the climate system. Quat. Sci. Rev. 22, 1821–1834.
Tegen, I., Heinold, B., Todd, M., Helmert, J., Washington, R., Dubovik, O., 2006. Modelling soil dust aerosol in the Bodélé depression during the BoDEx campaign. Atmos. Chem. Phys. 6, 4345–4359.
Tierney, J.E., Lewis, S.C., Cook, B.I., LeGrande, A.N., Schmidt, G.A., 2011. Model, proxy and isotopic perspectives on the east african Humid Period. Earth Planet Sci. Lett. 307, 103–112.
Todd, M.C., Bou Karam, D., Cavazos, C., Bouet, C., Heinold, B., Baldasano, J.M., Cautenet, G., Koren, I., Perez, C., Solmon, F., Tegen, I., Tulet, P., Washington, R., Zakey, A., 2008. Quantifying uncertainty in estimates of mineral dust flux: an intercomparison of model performance over the Bodélé Depression, northern Chad. J. Geophys. Res. Atmos. 113, D24107.
Todd, M.C., Washington, R., Martins, J.V., Dubovik, O., Lizcano, G., M'Bainayel, S., Engelstaedter, S., 2007. Mineral dust emission from the Bodélé depression, northern Chad, during BoDEx 2005. J. Geophys. Res. Atmos. 112.
Újvári, G., Klötzli, U., Stevens, T., Svensson, A., Ludwig, P., Vennemann, T., Gier, S., Horschinegg, M., Palcsu, L., Hippler, D., 2022. Greenland ice core record of last glacial dust sources and atmospheric circulation. J. Geophys. Res. Atmos., e2022JD036597
van der Does, M., Brummer, G.-J.A., Korte, L.F., Stuut, J.-B.W., 2021. Seasonality in saharan dust across the Atlantic Ocean: from atmospheric transport to seafloor deposition. J. Geophys. Res. Atmos. 126, e2021JD034614.
van der Does, M., Pourmand, A., Sharifi, A., Stuut, J.-B.W., 2018. North African mineral dust across the tropical Atlantic Ocean: insights from dust particle size, radiogenic Sr-Nd-Hf isotopes and rare earth elements (REE). Aeolian Research 33, 106–116.
Washington, R., Todd, M.C., 2005. Atmospheric controls on mineral dust emission from the Bodélé Depression, Chad: the role of the low level jet. Geophys. Res. Lett. 32, L17701.
Washington, R., Todd, M.C., Engelstaedter, S., Mbainayel, S., Mitchell, F., 2006a. Dust and the low-level circulation over the Bodélé depression, Chad: observations from BoDEx 2005. J. Geophys. Res. Atmos. 111, D03201.
Washington, R., Todd, M.C., Lizcano, G., Tegen, I., Flamant, C., Koren, I., Ginoux, P., Engelstaedter, S., Bristow, C.S., Zender, C.S., Goudie, A.S., Warren, A., Prospero, J.M., 2006b. Links between topography, wind, deflation, lakes and dust: the case of the Bodélé Depression, Chad. Geophys. Res. Lett. 33, L09401.
Yang, X., Liu, Y., Li, C., Song, Y., Zhu, H., Jin, X., 2007a. Rare earth elements of aeolian deposits in Northern China and their implications for determining the provenance of dust storms in Beijing. Geomorphology 87, 365–377.
Yang, X., Zhu, B., White, P.D., 2007b. Provenance of aeolian sediment in the Taklamakan Desert of western China, inferred from REE and major-elemental data. Quat. Int. 175, 71–85.
Ye, J., Chardon, D., Rouby, D., Guillocheau, F., Dall'asta, M., Ferry, J.-N., Broucke, O., 2017. Paleogeographic and structural evolution of northwestern Africa and its Atlantic margins since the early Mesozoic. Geosphere 13, 1254–1284.
Yu, H., Chin, M., Bian, H., Yuan, T., Prospero, J.M., Omar, A.H., Remer, L.A., Winker, D.M., Yang, Y., Zhang, Y., Zhang, Z., 2015a. Quantification of trans-Atlantic dust transport from seven-year (2007–2013) record of CALIPSO lidar measurements. Rem. Sens. Environ. 159, 232–249.
Yu, H., Chin, M., Yuan, T., Bian, H., Remer, L.A., Prospero, J.M., Omar, A., Winkr, D., Yang, Y., Zhang, Y., Zhang, Z., Zhao, C., 2015b. The fertilizing role of African dust in the Amazon rainforest: a first multiyear assessment based on data from cloud-aerosol Lidar and infrared pathfinder sateliite observations. Geophys. Res. Lett. 42, 1–8.
Yu, Y., Kalashnikova, O.V., Garay, M.J., Lee, H., Notaro, M., 2018. Identification and characterization of dust source regions ccross North Africa and the Middle East using MISR satellite observations. Geophys. Res. Lett. 45, 6690–6701.
Yu, Y., Kalashnikova, O.V., Garay, M.J., Lee, H., Notaro, M., Campbell, J.R., Marquis, J., Ginoux, P., Okin, G.S., 2020. Disproving the Bodélé depression as the primary source of dust fertilizing the amazon rainforest. Geophys. Res. Lett. 47, e2020GL088020.
Zabel, M., Schneider, R.R., Wagner, T., Adegbie, A.T., de Vries, U., Kolonic, S., 2001. Late quaternary climate changes in central Africa as inferred from terrigenous input to the Niger fan. Quat. Res. 56, 207–217.
Zhao, W., Balsam, W., Williams, E., Long, X., Ji, J., 2018. Sr–Nd–Hf isotopic fingerprinting of transatlantic dust derived from North Africa. Earth Planet Sci. Lett. 486, 23–31.